J. Fluid Mech. (1999), *vol.* 378, *pp.* 197–232. Printed in the United Kingdom

Laboratory observations of wave group evolution, including breaking effects

By MARSHALL P. TULIN AND TAKUJI WASEDA†
Ocean Engineering Laboratory, University of California Santa Barbara, CA93106

(Received 17 October 1997 and in revised form 11 August 1998)

The nonlinear evolution of deep-water wave groups, which are initiated by unstable three-wave systems, have been observed in a large wave tank (50 m long, 4.2 m wide, 2.1 m deep), equipped with a programmable, high-resolution wave generator. A large number of experiments were conducted (over 80 cases) for waves 1.0–4.0 m long, initial steepness $\epsilon = 0.10$–0.28, and normalized sideband frequency differences, $\delta\omega/\epsilon\omega$, 0.2–1.4. Using an array of eight high-resolution wave wires distributed in range (up to 43 m fetch), spectral evolution was studied in detail including the effect of background disturbances on the evolution. Minimizing those, new observations were made which extend the pioneering work of Lake *et al.* (1977) and of Melville (1982). Foremost, near recurrence without downshifting was observed without breaking, despite a significant but reversible energy transfer to the lower sideband at peak modulation; complete recurrence was prevented by the spreading of discretized energy to higher frequencies. Strong breaking was found to increase the transfer of energy from the higher to the lower sideband and to render that transfer irreversible. The end state of the evolution following strong breaking is an effective downshifting of the spectral energy, where the lower and the carrier wave amplitudes nearly coincide; the further evolution of this almost two-wave system was not studied here. Breaking during strong modulation was observed not only for the fastest growing initial condition, but over a wide parameter range. An explanation of the sideband behaviour in both the breaking and non-breaking case was given based on wave energy and momentum considerations, including the separate effects of energy and momentum loss due to breaking, and transfer to discretized higher frequencies throughout the spectra. Attention was drawn to the latter, which was almost universally observed.

1. Introduction

Since Benjamin & Feir (1967) showed theoretically and experimentally that the Stokes' wave was unstable to modulational perturbations, a number of other experimental investigations have been conducted on the long-time evolution of nonlinear wave trains, see table 1. Certain findings have greatly contributed to advancing the nonlinear science of deep-water gravity waves. The range of parameters and conditions in the past experiments were however limited. Note that most of the experiments were conducted for a range of steepness, but with a single fixed or naturally determined modulational frequency. Short waves (<1.0 m) were also typically used, since the sideband evolution is a slow process with time scale inversely proportional to the square of the steepness, and tank lengths were limited. The shortcoming of using

† Present address: The International Pacific Research Center, University of Hawaii, HI 96822, USA.

Experiment	Tank	λ	ϵ	$\delta\omega/\omega_0$
BF*	42 m	2.16 m	0.17	0.15
		0.25 m	0.07–0.15	**0.1**
LYRF*	0.9×0.9×12 m	12–70 cm	0.1–0.35	**0.1, 0.2**
RM	3×1×40 m	1.0 m	NA	∼0.25
S*	100×0.8×340 m	0.6–1.3 m	0.09–0.34	$O(\epsilon)$
	3.66×3.66×137 m			
M*	0.5×0.6×28(16) m	0.4 m	0.2–0.3	$O(\epsilon)$
BR	2.6×1.0×100 m	0.8 m	∼0.24	NA
BHL	1.0×0.75×20 m	0.4 m	0.1–0.2	$O(\epsilon)$
OEL	4.2×2.1×50 m	1.0–4.0 m	0.10–0.28	$\mathbf{0.2}\epsilon\sim\mathbf{1.4}\epsilon$

TABLE 1. A list of modulational instability experiments performed in the past; bold face letters indicate that the modulation was imposed on the wave-generator motion. BF: Benjamin & Feir (1967), LYRF: Lake *et al.* (1977), RM: Ramamonjiarisoa & Mollo-Christensen (1979), S: Su, Bergin, Marler & Myrick (1982) and Su (1982), M: Melville (1982), BR: Bonmarin & Ramamonjiarisoa (1985), BHL: Bliven, Huang & Long (1986), OEL: this study

short waves is that the effect of surface tension is no longer negligible in regions near the highly deformed wave crest for waves below about 1 m in length. For waves shorter than 60–70 cm, non-splashing 'micro-breakers' appear, see figure 10 of Melville (1982), rather than energetic splashing jets as in the case of waves over 1 m in length, see figures 10 and 12; differences in evolution due to these different breaking regimes have never been quantified. In addition, the width of the tanks used in the past was limited and can significantly affect evolution due to small but significant sidewall damping; this was already noted by Benjamin (1967).

Except in a few cases, most experiments were conducted without perturbing an otherwise monochromatic wave-generator motion. The modulation therefore naturally evolved from background noise and the modulational frequencies were thus naturally determined. We call these 'un-seeded' experiments. On the other hand, if the modulation is imposed at the wave generator, it is possible to change not only the sideband frequencies at will, but also the initial sideband amplitudes and the strength of the modulation. We call this a 'seeded' experiment. The differences arising between 'seeded' and 'un-seeded' experiments will be discussed briefly in §3.2.

Among the past works listed in table 1, those of Benjamin & Feir (1967), Lake *et al.* (1977), Su & Green (1985), and Melville (1982), denoted by an asterisk in table 1, have a direct connection with the work presented in this report. In particular, the work of Lake *et al.* and Melville is particularly relevant, and they have, indeed, inspired the present investigation.

In a remarkable, ground breaking paper, Lake *et al.* (1977) have studied experimentally and numerically the long-time evolution of nonlinear wave trains, and discovered that evolution occurs in recurrent fashion, where the modulation periodically increases and decreases, the wave form returning periodically to its previous form. Although a complete recurrence was theoretically demonstrated in their paper through a numerical solution of the nonlinear Schrödinger (NLS) equation, their experimental results were ambiguous and somewhat contradictory.

In their experimental example at small steepness ($\epsilon \sim 0.1$), the wave envelope modulated and the spectral bandwidth broadened at peak modulation, displaying a number of high-frequency peaks. Past peak modulation, the wave envelope demodulated and the spectral bandwidth reduced as the high-frequency spectral content

diminished. Thus, the original near three-wave system was almost recovered, but with an important exception: the spectral peak downshifted to a lower sideband, despite the absence of breaking.

In their other example at a higher steepness ($\epsilon = 0.2$) breaking occurred at the peak modulation. When the wave train demodulated, the number of waves per group as well as the group period itself did not change, indicating that significant energy was not shifted to the lower sideband. These two experiments clearly contradicted each other as to whether breaking or downshifting does or does not occur during evolution. These experiments are also ambiguous as to whether recurrence (no downshifting) is a consequence of evolution in a conservative system, as predicted by their NLS computations.

Following Lake *et al.*'s work, Melville (1982) conducted a series of sideband evolution experiments, all containing breaking events, unquestionably to answer some of the troubling and important questions left over. Melville's conclusion was that 'the evolution of the spectrum is not restricted to a few discrete frequencies but also involves a growing continuous spectrum, and the description of the evolution as a recurrence phenomenon is incomplete'. He suggests that the end state of the evolution is inevitably a breaking event, followed by partial recurrence tending to lower frequency. Melville did not observe any recurrence of Fermi–Pasta–Ulam type, but the initial wave steepness he used was over $\epsilon = 0.2$, much higher than those used by Lake *et al.*

Unfortunately, these two pioneering studies have not been followed by further systematic measurements and analyses to pursue the various questions they raise. For example: no one has demonstrated even near-recurrence in the absence of breaking as predicted by Lake *et al.*; the mechanisms underlying lower sideband behaviour have not been elucidated, and particularly the relative roles of conservative versus breaking processes; Melville's 'growing continuous spectrum' has not been confirmed or further studied; measurements of evolution during breaking and of the limits of breaking have not been made. Therefore, in order to understand the behaviour of evolving wave groups with less ambiguity and to cover a much wider parameter space, we have conducted a 'seeded' experiment for waves with lengths in the range of 1–4 m, initial steepness $\epsilon = 0.1$–0.28, and 'seeded' modulational frequencies $\delta\omega/\omega = (0.1\text{–}1.5)\epsilon$. The initial sideband amplitudes $b_{\pm}/a$ were also varied. Special care was taken in order to minimize the effect of background disturbances in the tank. It is, to our knowledge, the first systematic experiment on the evolving wave train using long waves in a large wave tank, and it indicated the advantage of 'seeded' over 'un-seeded' experiments. The results directly relate to important questions following the previous pioneering work of Lake *et al.* and Melville.

In §2, some of the theoretical background of the subject is summarized with information helpful in designing an instability experiment. Section 3 describes the facility and the experimental procedure in detail including effects of tank background disturbances on wave train evolution. In §4, experimental results are presented from the sideband wave evolution experiments including breaking and non-breaking evolution; §5 contains a discussion of the results including a theoretical development which provides an explanation for the effect of breaking on downshifting as well as the role of energy transferred to higher frequencies. Section 6 contains brief concluding remarks.

2. Theoretical background

The focus here is on a simple summary of theoretical results. Readers who are interested in a more detailed review on the subject should refer to comprehensive review articles by Yuen & Lake (1980) and by Hammack & Henderson (1993).

Benjamin & Feir (1967) performed a perturbation analysis of the uniform wave train based on the Euler equations and showed that a wave train with initial amplitude a_0, wavenumber k_0, and frequency ω_0 is unstable to perturbations with frequency $\delta\omega$, when the following condition is satisfied:

$$0 < \hat{\delta} \leqslant \sqrt{2}, \tag{2.1}$$

where $\hat{\delta} \equiv \delta\omega/\epsilon\omega_0$ and $\epsilon \equiv a_0 k_0$. The modulational instability is an interaction among three monochromatic wave trains: carrier (ω_0), upper (ω_+), and lower (ω_-) sideband waves, that satisfy the following conditions:

$$\left.\begin{aligned} 2\omega_0 &= \omega_+ + \omega_-, \\ \omega_\pm &= \omega_0 \pm \delta\omega, \\ 2k_0 &= k_+ + k_- + \Delta k, \end{aligned}\right\} \tag{2.2}$$

where Δk is a slight mismatch of the wavenumber from Phillips' four wave resonance conditions for infinitesimal waves. Due to the cancellation of this resonant de-tuning in the presence of amplitude dispersion, sideband waves grow exponentially (Phillips 1967), and the growth rate $\mathrm{d}(\ln a)/\mathrm{d}(kx)$ as predicted by Benjamin & Feir (1967) is

$$\beta = \epsilon^2 \hat{\delta}(2 - \hat{\delta}^2)^{1/2}. \tag{2.3}$$

Maximum growth is produced for $\hat{\delta} = 1.0$ and for the initial phases of the sidebands $\phi_\pm = -\frac{1}{4}\pi$.

Lake *et al.* (1977) have conducted a controlled experiment in a laboratory tank, and compared the various characteristics of the evolution of the nonlinear wave train with the numerical solution of the nonlinear Schrödinger equation (Zakharov 1968; Chu & Mei 1970). Although the initial growth rate as obtained through the numerical solution of the NLS equation agreed with the theoretical prediction by Benjamin & Feir (1967), the experimentally determined growth rate required an artificial correction to the empirically determined steepness for agreement with Benjamin & Feir's theoretical predictions (Lake & Yuen 1977). The correction was fictitious (Yuen & Lake 1982), and a later study indicated that the theories, rather than the experimental result itself, had to be improved. Dysthe (1979) has undertaken this task, and derived a correction term for the NLS equation, extending it to broader bandwidths; it has been claimed that the higher-order-term correction introduced here is strictly due to the broader bandwidth assumption and not due to the correction in amplitude, Stiassnie (1984). Dysthe's equation was solved numerically (Lo & Mei 1985) for the long-term evolution of nonlinear wave trains, and showed an asymmetric growth of the sidebands, the lower growing at the expense of the upper. The numerical method first introduced by Lo & Mei (1985) and later improved by Trulsen (1989) has proved to be very efficient and easy for numerically implementing Dysthe's equation. However, the steepness range of validity is still limited ($\epsilon < 0.10$) as seen in the comparison of the predicted fastest growing modulational frequencies with the exact result of Longuet-Higgins (1980) (see figure 16). Yuen & Lake (1982) have suggested the use of the so-called Zakharov integral equation Zakharov (1968). They have successfully solved the equation and derived the growth rates for a one-dimensional modulation showing a better agreement with experimental results for moderate steepness ($\epsilon = 0.10$ and higher) than given originally by Benjamin & Feir (1967).

There are some limitations in previous Zakharov-based calculations and therefore we have undertaken improvements based on Krasitskii's reduced four-wave interaction equation Krasitskii (1994), which is a very useful modification of the Zakharov integral

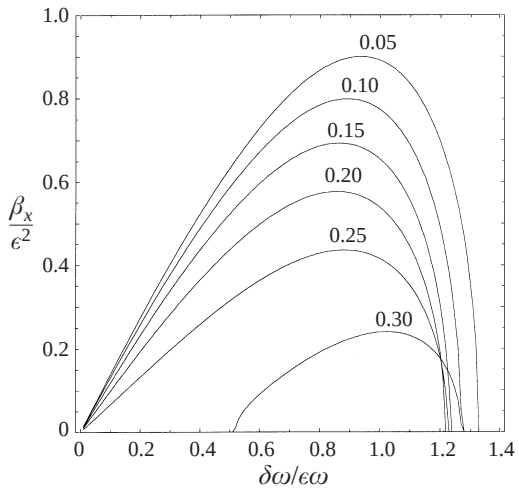

FIGURE 1. Initial growth rate, β_x, of the sideband disturbance, based on Krasitskii's reduced four-wave interaction equation (Krasitskii 1994). The curves are for steepness $\epsilon = 0.05$, 0.10, 0.15, 0.20, 0.25 and 0.30, plotted against normalized modulational frequency $\delta\omega/\epsilon\omega$.

equation. Figure 1 displays the growth rate computed by us, based on Krasitskii (1994). It leads easily to the determination of the $\hat{\delta}$-range giving the largest growth rate for given ϵ. Such a diagram is very useful when planning experiments such as are reported here, where the full evolution is to be studied, well beyond the range of instability theory. Oshri (1996) has numerically implemented these same Krasitskii's Hamiltonian equations and studied the evolution of the unstable Stokes' wave including non-conservative effects due to wind input and dissipation.

Fully nonlinear computations have also been applied to the study of the long time evolution of unstable Stokes' waves: Dold & Peregrine (1986); Dommermuth & Yue (1987); Tulin *et al.* (1994); Landrini *et al.* (1998). The problem is solved for a periodic spatial domain except in Tulin *et al.* (1994), which is a numerical wave tank, called LONGTANK, wherein the exact inviscid flow in the wave tank including exact wavemaker shape and motion is simulated in time. Direct comparisons of wave elevation time series between LONGTANK and experimental observations are possible up to the point of wave breaking, beyond which the computation must stop. Such a comparison is shown in figure 2. Time series obtained from a wave wire range along the length of the Ocean Engineering Laboratory (OEL) tank is compared with LONGTANK simulations; the waves were generated by the wavemaker starting at rest. The dotted line (measurements) overlaps the LONGTANK simulation (solid line) to such an extent that it is difficult to separate the two curves up to breaking, beyond which the simulations cease. The prediction of breaking was also observed to be close.

In a separate work, Landrini *et al.* (1998), we have carried out an extensive study comparing a variety of weakly nonlinear models (Krasitskii, Dysthe and NLS) with high-resolution fully nonlinear computations. Using the fully nonlinear computations as a baseline this study compared the success of the other models in predicting evolution through several cycles of recurrence and found their rank order of success to be Krasitskii, Dysthe, NLS; the success of Krasitskii depended upon using a sufficient number of wave modes. All of these simulations, except NLS, confirm the major features of the near recurrence experiment reported here: an increase of energy in the lower sideband relative to the upper as the peak modulation is approached

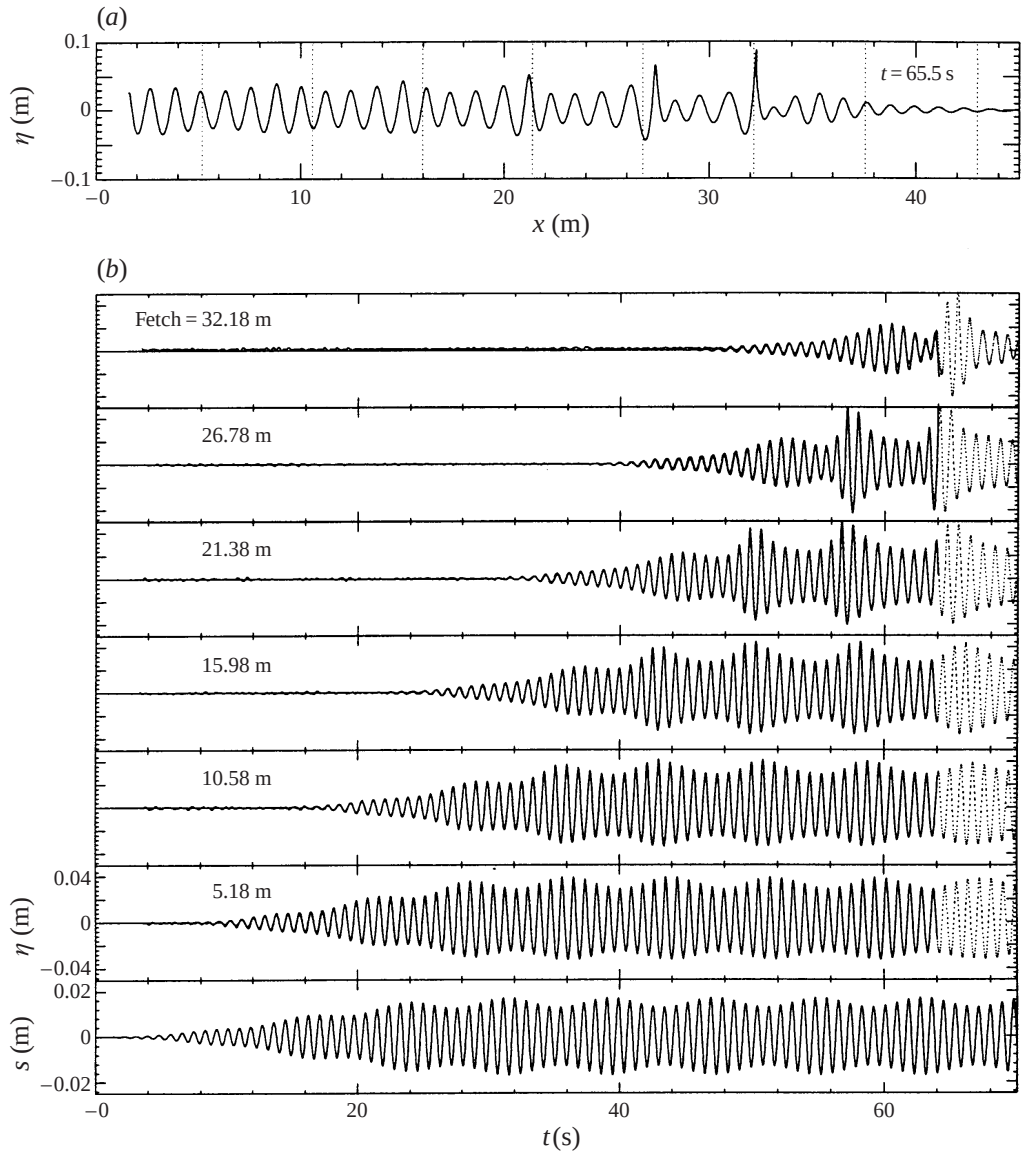

FIGURE 2. Comparison of the fully nonlinear model (LONGTANK) and the experimental observation. Solid line: LONGTANK, dotted line: experiment. (*b*) The time series of the surface elevation at fetches 5.18, 10.58, 15.98, 21.38, 26.78 and 32.18 m, and the time series of the plunger motion. (*a*) The spatial surface elevation snapshot from LONGTANK, showing the wave breaking at a fetch of 32.18 m.

followed by the disappearance of that difference in energies as recurrence progresses. The fully nonlinear simulation showed breaking, when it occurs, close to the peak in the modulation.

In figure 2, the time traces from the wires closest to the wavemaker (*b*) show a regular modulation corresponding to the weak sidebands which have grown to that location. At subsequent locations the modulations grow in amplitude due to sideband growth and finally (*a*) the groups become asymmetric about the crests, the group front steepening due to unequal sideband growth, culminating in breaking. In figure 3

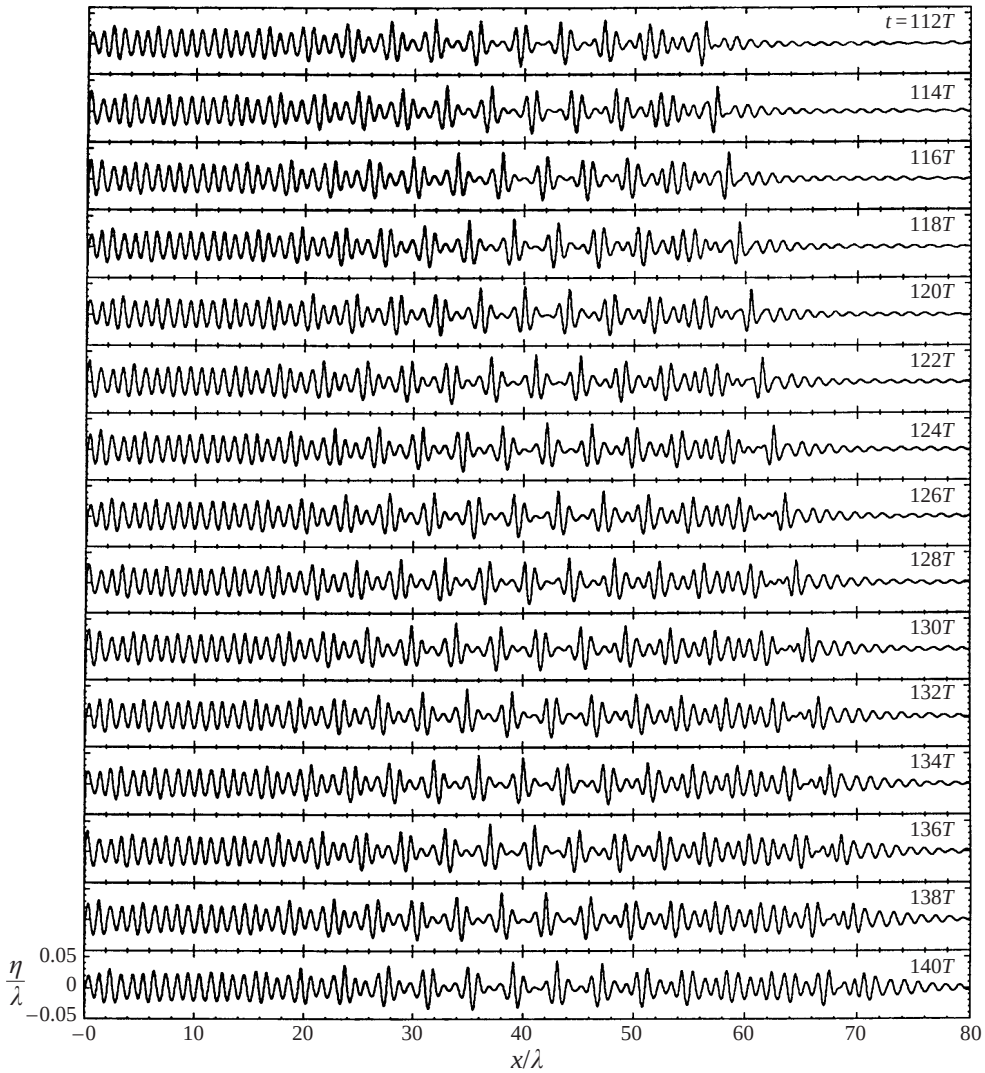

FIGURE 3. Spatial surface elevation snapshots at different times obtained from LONGTANK simulation showing tendency toward recurrence.

is another LONGTANK simulation without breaking showing the tendency to recurrence (compare with figure 9(*c*)) and figure 4 from a breaking case, the details of breaking showing the concave front face and jet development, just as observed and pictured in figure 12. Unfortunately, the LONGTANK simulations, being inviscid, cannot include effects of real dissipation following jet splash, which must be studied through tests like these.

A discussion of downshifting which is relevant for understanding the experimental results reported here was presented by Tulin (1996). Through global considerations of both wave energy and momentum conservation in a multi-modal wave system evolving from a carrier wave and two sidebands, he showed the specific role which both momentum losses and energy dissipation play in determining the shifting of energy between sidebands. In particular he showed that it is not dissipation alone

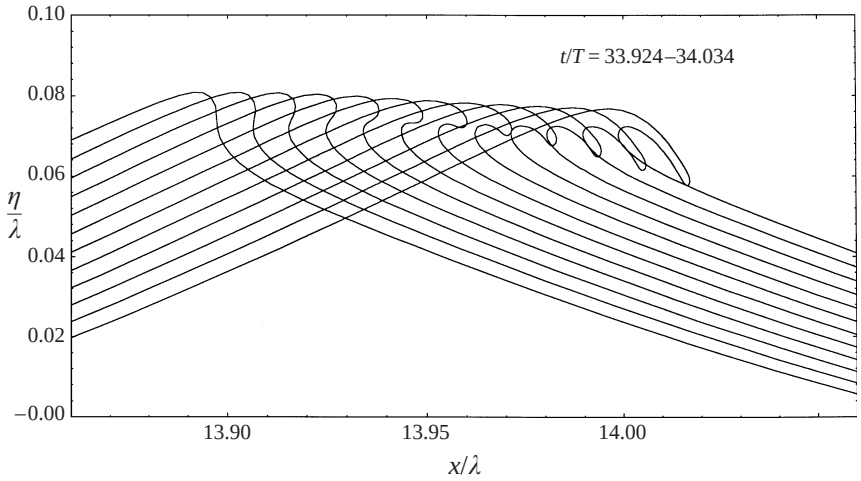

FIGURE 4. LONGTANK simulation of the breaking event, showing the plunging jet development.

which determines downshifting, but the balance between momentum and dissipation losses, suitably parameterized. His brief demonstration is extended in §5.3 of this paper to include the role of nonlinear energy transfer between modes, especially to higher frequencies. The latter transfers provide the basic mechanism for downshifting in the absence of breaking dissipation, but they are substantially reversible, therefore accounting for the observed reversal of downshifting past the modulation peak. The original discussion of Tulin (1996) includes a parameterization of both the energy and momentum loss in the jet accompanying breaking.

3. Facility and experiments

3.1. *Facility*

The tank is 50 m length, 4.2 m wide, 2.1 m deep with a 30 m wind tunnel section of 1.5 m air passage height. In an upwind view of the tank, figure 5, several steep waves breaking energetically at the peak of wave groups can be seen. The wave generator, designed and constructed within the OEL, is a plunging type driven by two parallel hydraulic pistons. The dimension of the plunger is about 4.2 m wide, 2 m long, and 1 m deep. The plunger has a detachable front face section made of Styrofoam, optimized for generating planar waves in the range of 60 cm to 10 m lengths. The plunger shape was designed as part of a systematic study of wave making in a narrow tank by Yao (1992).

FIGURE 5. Ocean Engineering Laboratory (UCSB) wind-wave tank. Facility. Wavemaker: computer-driven bi-modal plunger with interchangable front faces; $\lambda \sim 0.6$–10 m and maximum wave height of 0.64 m (frequency dependent). Wind tunnel: maximum flow rate of 13 m s^{-1} (off- and onshore capabilities). Tow Carriages: surface and sub-surface carriages capable of maximum speeds of 5 m s^{-1} and 1 m s^{-1} respectively. Instrumentation. FMCW Radar: 4–8 GHz, dual polarization, pulse repetition rate 500 Hz. High-speed video camera: CCD array of 256×256 pixels; maximum frame rate 1000 Hz. Wave profile measurement: capacitance-type wave wires with 1 kHz sample frequency and resolution of 0.5 mm per m wire length. Flow measurement: 3-axis acoustic Doppler velocimeter. Wind measurement: 2-channel hot-film anemometer and pitot tubes. Light box: for surface visualization and quantitative measurement of wave slopes over 1 m square.

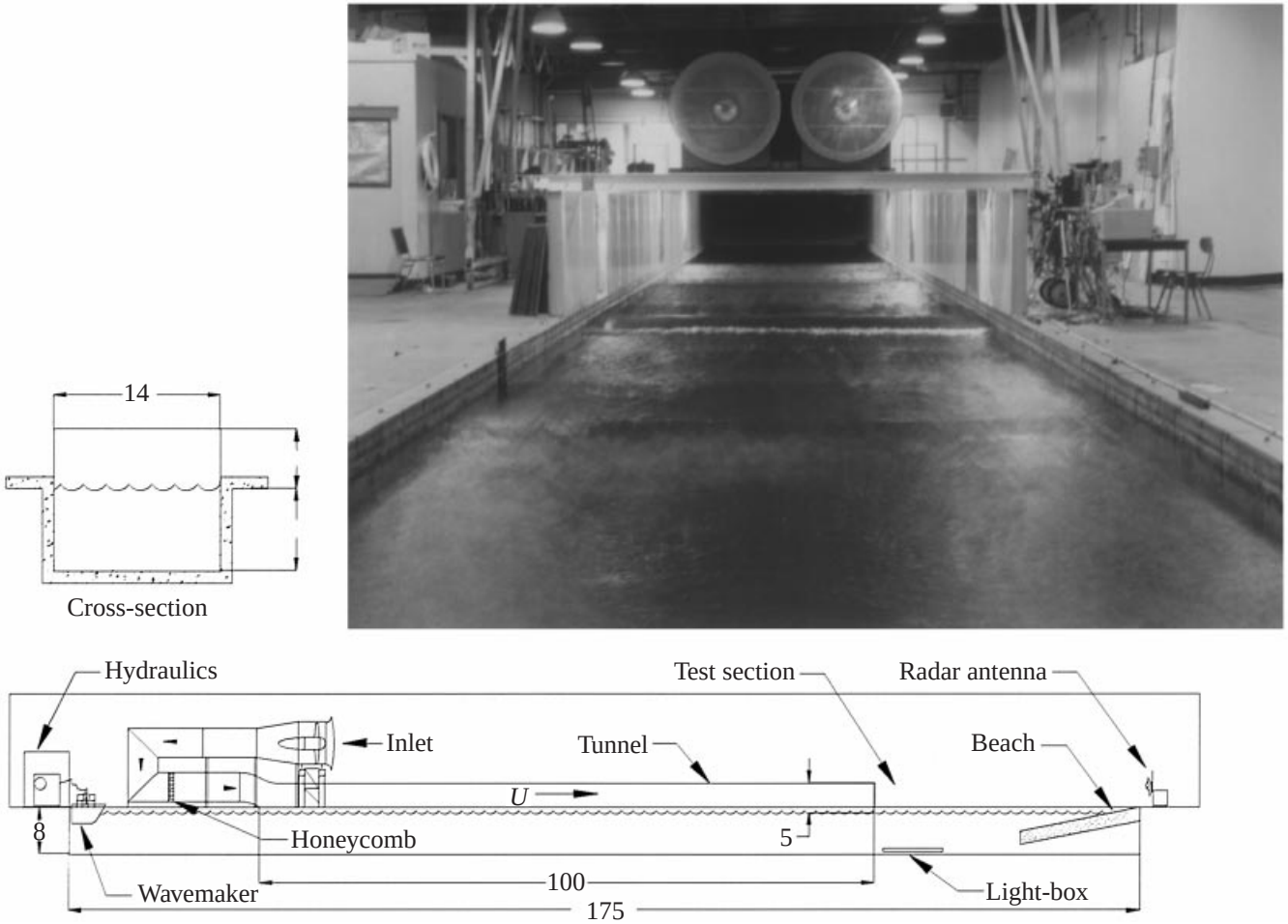

FIGURE 5. For caption see facing page.

The motion of the plunger is controlled by a programmable controller made by MTS inc. The controller takes an external input signal for the motion generated by a 486PC. The signal is generated by the National Instrument LabVIEW transmitted through a digital communication interface. The 15 bit signal at 200 Hz can be either generated in real time or read from a data file stored on the hard disk. The frequency response of the plunger was measured by a position feedback at the wave generator. As a result, a frequency-dependent transfer function of counts (0–2^{15}) to the actual stroke of the plunger was obtained. The stroke was then compared with the actual wave amplitude measured at the wave tank with the wave wire. The stroke and the wave amplitude ratios are nearly constant for waves longer than 1.5 m.

3.2. *Source of background disturbances in the tank*

Background noise anywhere in the system can seed a selective amplification of some wave components in resonant interaction experiments (Hammack & Henderson 1993). In order to conduct a controlled resonant interaction experiment, it is therefore necessary to minimize important sources of disturbance.

Wave reflection from the beach does not have an immediate influence on amplification and phase shifting of the incoming wave in the region of measurements, since the energy reflection coefficients (energy of the reflected wave/energy of the incoming wave) of our waves (1.0–4.0 m) were measured to be only about 0.1 %. However, long duration experiments showed that the most significant source of background noise is associated with the wave front of the propagating wave train and its multiple reflections from the beach; the multiple reflections of this wave front between the beach and the wave-generator after a long time create initial sidebands through selective amplification by the wave system; this was first observed by Melville (1982). Cross-tank wave modes also cause important disturbances since they introduce an ambiguity in wave measurement due to cross-tank bias; it is noticeable that breaking waves become more three-dimensional due to a small standing wave mode across the tank. The effect of wall dissipation may not be neglected if the sideband growth rate is small. These noise sources have all been described in detail in Waseda (1997).

3.2.1. *Multiple reflections of the wave front, and effects of seeding*

Figure 6 shows the long time evolution of the envelope of initially monochromatic 1 m waves where the sideband disturbances were not imposed on the wave-generator motion ('un-seeded'). The diagonal line indicates the travel path of the wave front of the wave train propagating at the group speed. Observe that only after several round-trips of the wave front does the wave envelope start to modulate and that modulation is clearly associated with the travel path of the wave front, see figure 6. This strongly suggests that the source of modulational disturbances lies in a disturbance travelling with the front of the wave train at the group speed. The resulting modulational frequency roughly corresponds to the peak region of the growth curves predicted by instability theories (figure 1), but not necessarily the fastest growing one. The initial sideband amplitudes $b_{\pm}/a_0$, are unpredictable and probably strongly depend on the characteristics of the tank.

Figure 7 compares the spectral evolution of an 'un-seeded' and 'seeded' run. In the 'un-seeded' case, (*a*), the sideband modes grew with fetch, but the spectral peaks are broad. At earlier fetches, we may even find multiple peaks around the sideband modes. Our interpretation of this broadening is that the frequencies of the naturally grown sideband disturbances change in a certain range with time, perhaps stochastically under the influence of noise in the water, and that therefore the spectral peak

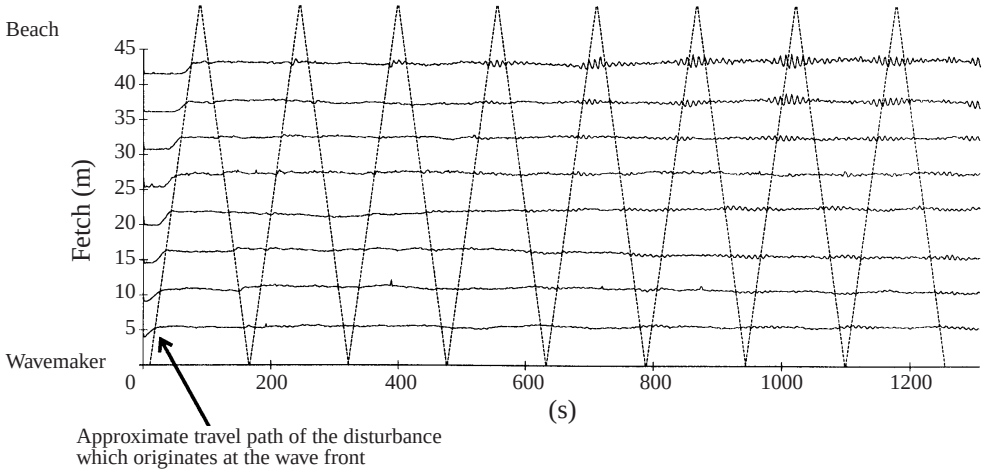

FIGURE 6. Long time evolution of the wave envelope; diagonal line indicates the multiple reflection of the wave front. $\lambda = 1.0$ m (1.23 Hz), $\epsilon = 0.096$. The envelope was obtained by means of the Hilbert transform.

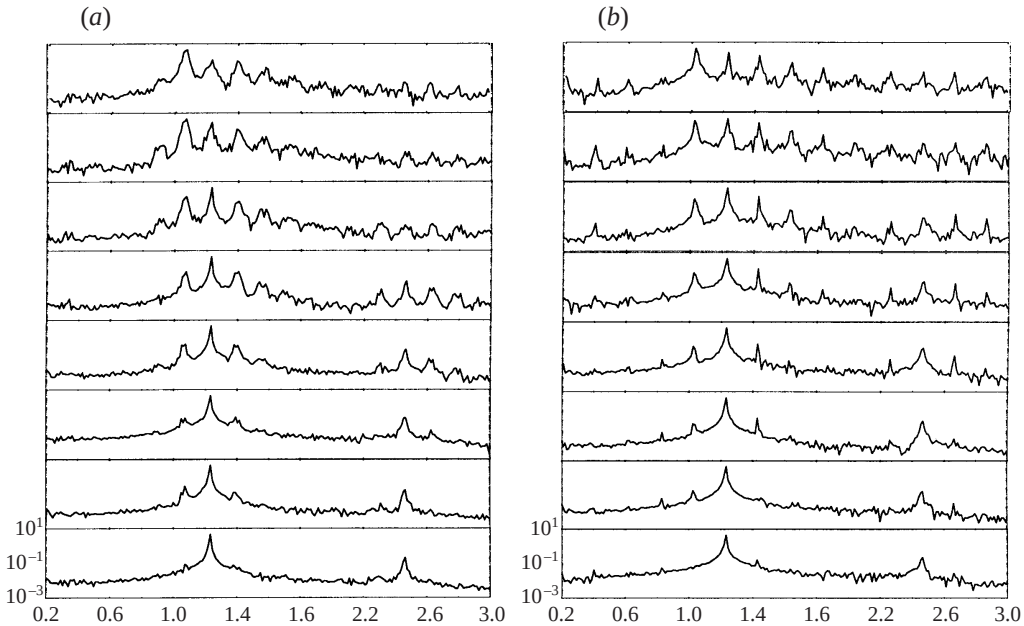

FIGURE 7. Spectral evolution of modulated wave train. (*a*) No modulation imposed on the wave-generator motion. $\lambda = 1.0$ m (1.23 Hz), $\epsilon = 0.162$. Naturally appearing sideband frequencies are around 1.39 Hz and 1.07 Hz. (*b*) Modulation imposed on the wave-generator motion. $\lambda = 1.0$ m (1.23 Hz), $\epsilon = 0.162$. Sideband frequencies: 1.43 Hz and 1.03 Hz, $a_{\pm}/a_0 = 0.02$. Fetches; 3.6 m, 9.0 m, 14.4 m, 19.8 m, 25.2 m, 30.6 m, 36 m, and 41.4 m from bottom to top. Four degrees of freedom.

of the ensemble-averaged spectrum broadens. The naturally evolving modulational frequency in the case of figure 7 corresponds to $\hat{\delta} = 0.8$, which is close to but slightly smaller than the fastest growing condition at $\epsilon = 0.163$, $\hat{\delta} \sim 0.86$, see figure 1. The selection mechanism for the modulational frequency of the 'un-seeded' experiment

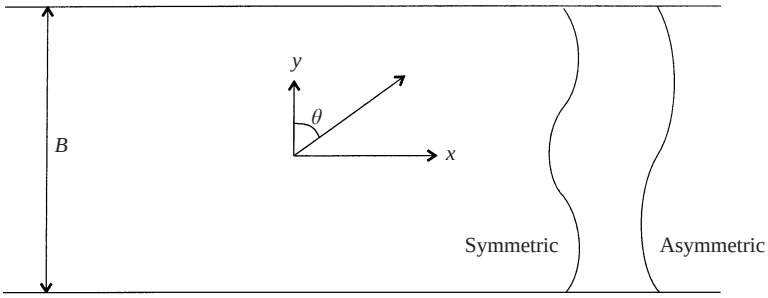

FIGURE 8. Schematics describing the cross-tank wave mode in a narrow wave tank.

probably contains both stochastic and deterministic features depending among other things on the tank geometry. This introduces an ambiguity in the experiment. Since the development of the sideband in the 'un-seeded' case takes time, in order to study the evolution of the modulational wave train it is necessary to wait for as long as 20 min (Melville 1982) until the starting transients disappear. Therefore, the subsequent experiments are carried out in a relatively noisy environment.

On the other hand, the modulational characteristic of the 'seeded' case, (*b*), is seen to be stable; the sideband frequency is locked to the modulational frequency imposed at the wave generator. Such comparisons suggest that imposing the modulation on the wave-generator motion is advantageous for studying wave group evolution in itself, since it reduces experimental ambiguity by allowing experiments to be conducted prior to the growth of noise from the continual passage of the wave front, i.e. within the first 5 min of operation. This technique therefore allows full control of the parameter values $\delta\omega$ and $b_{\pm}/a$, less noise, and therefore better conditions for comparison with theory. Of course, the natural selection process and noise effects are of interest in their own right. We have used both processes in systematic studies of wind effects on initial instability growth, which will be reported elsewhere.

3.2.2. *Three-dimensionality in the tank*

Although the reflected wave energy from the beach is small, it is a source of cross-tank wave disturbances since the reflected disturbance can be three-dimensional.

Due to well known waveguide effects (Yao, Tulin & Kolaini 1994), waves shorter than twice the tank width can propagate down-tank at an angle θ only if they satisfy the following relation:

$$k\cos(\theta) = \begin{cases} k_B\, n & \text{symmetric mode} \\ k_B\, n/2 & \text{asymmetric mode,} \end{cases} \tag{3.1}$$

where $k \equiv 2\pi/\lambda$, $k_B \equiv 2\pi/B$ (B is the breadth of the tank), and n is an integer (figure 8). Suppose a propagating wave mode $a\cos(kx - \omega t)$ and cross-tank wave modes $s\cos(k\,\sin\theta\, x \pm k\,\cos\theta\, y - \omega t)$ co-exist, the wave pattern in the tank will be

$$\eta = a\,\cos(kx - \omega t) + 2s\,\cos(k\sin\theta\, x - \omega t)\cos(k\,\cos\theta\, y). \tag{3.2}$$

For a given fetch x, the second term of (3.2) represents a standing wave pattern across the tank. This cross-tank mode vanishes when $\lambda \geqslant 2B$, according to (3.1).

Two wires were placed across the tank (fetch 27 m, at the centre and 1.4 m off the centre) in order to observe the development of the standing wave pattern. Starting from a uniform initial amplitude across the tank that occurs just after the wave generator was initiated (0.825 Hz monochromatic wave, 2.3 m), it took more

than 5 min until the cross-tank standing wave pattern developed and reached an equilibrium state. This time corresponds to about three to four round-trips of the waves within the tank. This suggests that in order to minimize the influence of cross-tank wave modes in the measurement, the wave-generator motion should terminate before the wave front makes 3–4 round-trips. Measurements were typically taken from the beginning of the wave generator initiation until after the termination of the wave generator, but the analyses were restricted to the segment of data containing the early part of the wave train where the influence of such disturbances are minimal.

3.2.3. *Energy dissipation at the sidewall*

The dissipation rate $\mathrm{d}(\ln a)/\mathrm{d}(kx)$ of the progressing deep water wave due to the dissipation at the wall boundary layer is found using Ursell's (1952) linearized theory with the result (Lo & Mei 1985)

$$\beta_D = \frac{(2\nu/\omega_0)^{1/2}}{B}, \tag{3.3}$$

which is not a function of the wave steepness ϵ.

For $\nu = 10^{-6}$ m^2 s^{-1}, and $B = 4.2$ m, the rate of dissipation β_D is $1.34 \times 10^{-4} \times f^{-0.5}$, where f is the frequency of the wave. The dissipation at the sidewall is negligible if the following condition is satisfied:

$$\hat{\delta}(2 - \hat{\delta}^2)^{1/2}\epsilon^2 \gg 1.34 \times 10^{-4} f^{-0.5}; \tag{3.4}$$

(3.4) was satisfied for all the experiments conducted here, but not in all previous experiments, listed in table 1.

3.3. *Wave-generator signal*

In a 'seeded' experiment, the derived wave train at its initial stage is

$$\eta = a_c \sin(\omega_0 t) + b_+ \sin(\omega_+ t + \phi_+) + b_- \sin(\omega_- t + \phi_-), \tag{3.5}$$

where ω_0, ω_+, and ω_- satisfy (2.2), and a_c, b_+, and b_- satisfy the following relation:

$$a_0^2 = a_c^2 + b_+^2 + b_-^2. \tag{3.6}$$

Here, a_0 is the amplitude of the equivalent unmodulated wave train with initial steepness $\epsilon \equiv a_0 k$. The initial phases ϕ_+ and ϕ_- were set to $-\frac{1}{4}\pi$, which is the maximum growth condition ($\phi_+ + \phi_- = -\frac{1}{2}\pi$) predicted by Benjamin & Feir (1967). Furthermore, b_+ and b_- were set equal. Therefore, the choices of parameters in (3.5) are a_0, b_+, and $\delta\omega$ or

$$\epsilon, \qquad b_+/a_0, \qquad \text{and} \qquad \hat{\delta}, \tag{3.7}$$

for a given wavelength.

In order to avoid the development of noise in the tank, the wave-generator motion was started and terminated with a finite ramp of duration τ. The actual wave-generator control signal used is

$$Y(t) = e(t)\frac{s}{2}\left[\frac{a_c}{a_0}\cos(\omega_c t) + \frac{b_+}{a_0}\cos(\omega_+ t + \phi_+) + \frac{b_-}{a_0}\cos(\omega_- t + \phi_-)\right], \tag{3.8}$$

where

$$e(t) = \begin{cases} \frac{1}{2}\left(1 - \cos(\pi t/\tau)\right), & 0 \leqslant t \leqslant \tau, \\ 1, & \tau < t < T - \tau \\ \frac{1}{2}\left(1 - \cos(\pi(t - T)/\tau)\right), & T - \tau \leqslant t \leqslant T, \end{cases} \tag{3.9}$$

where T is the total length of the data, and s is the stroke in arbitrary units. Note that if τ is too short, the starting wave front breaks before reaching the beach, which creates local disturbances and may not be desirable for certain experiments. We have avoided this effect.

4. Evolution results

4.1. *Evolution of recurrent type*

The experiment here is designed to repeat the conditions of the evolution experiment on a weak wave ($\epsilon \sim 0.1$) reported in Lake *et al.* (1977), but on a larger scale; the wavelength here is 1.0 m compared with 40 cm in Lake *et al.* The spatial development of the wave train, and the spectra are shown in figure 9. The wave lies outside the breaking regimes, as we discuss later. The maximum modulation is reached midway down the tank (25 m fetch). Discretized energy appears there over most of the visible spectrum at frequencies higher than the higher sideband, with frequency intervals of the order of $\delta\omega$. The asymmetric growth of $(b_- - b_+)$ is evident as well as the later tendency towards reversal. Ultimately a spectrum is recovered at a fetch of 41.4 m in which the greatest portion of the original energy still resides in the original three waves, with the carrier wave dominant. The recurrence here is, in fact, much closer to the NLS or three-wave prediction than found in Lake *et al.* at this steepness, since here there is neither a reduction in the number of waves per group nor downshifting of the spectral energy. Only at the peak modulation, at fetches 19.8 m and 25.2 m in figure 9(*c*), does the number of waves per group appear to have been temporarily reduced from 11 to 10; we return to this observation in §5.6.

Despite a tendency toward reversal during demodulation, at the end of the modulation cycle (41.4 m fetch) there is noticeable discretized high-frequency energy spread in the spectrum, broadening it, figure 9(*b*), particularly just below the higher sideband; the energy levels in these discretized spectra are very low, see figure 9(*a*). The failure of this discretized energy to be transferred back to the original three waves has prevented perfect recurrence. At the same time, there does not appear to be a tendency for the generation of a continuous spectrum, as suggested in Melville (1982).

It should be noted that the interpretation of the high-frequency portion of the spectrum, as in figure 9(*a,b*), must take into account the presence of a multiplicity of bound waves accompanying the free wave spectrum. These bound waves consist not only of the well known Stokes' harmonics for each free wave, but of sum (and difference) frequencies which arise from second-order interactions corresponding to each pair of free waves. It is all these bound waves which are probably responsible for the bulk of discretized spectral energy for frequencies beyond about midway between carrier and second harmonic frequencies; any additional energy there due to free waves created by nonlinear transfer cannot easily be identified.

Finally, in interpretation of the somewhat contradictory Lake *et al.* results, and especially the appearance of downshifting in the absence of breaking, it is worth noting that the estimated wave decay rate in their tank, due both to internal and wall dissipation, is 8% of the sideband growth rate (estimated), and could have influenced the dynamics of the modal interactions.

4.2. *Evolution with breaking and downshifting*

Two separate series of experiments have been conducted, involving over 80 runs, all seeded; breaking was of the plunging jet type. In the first series, utilizing 1.2 m

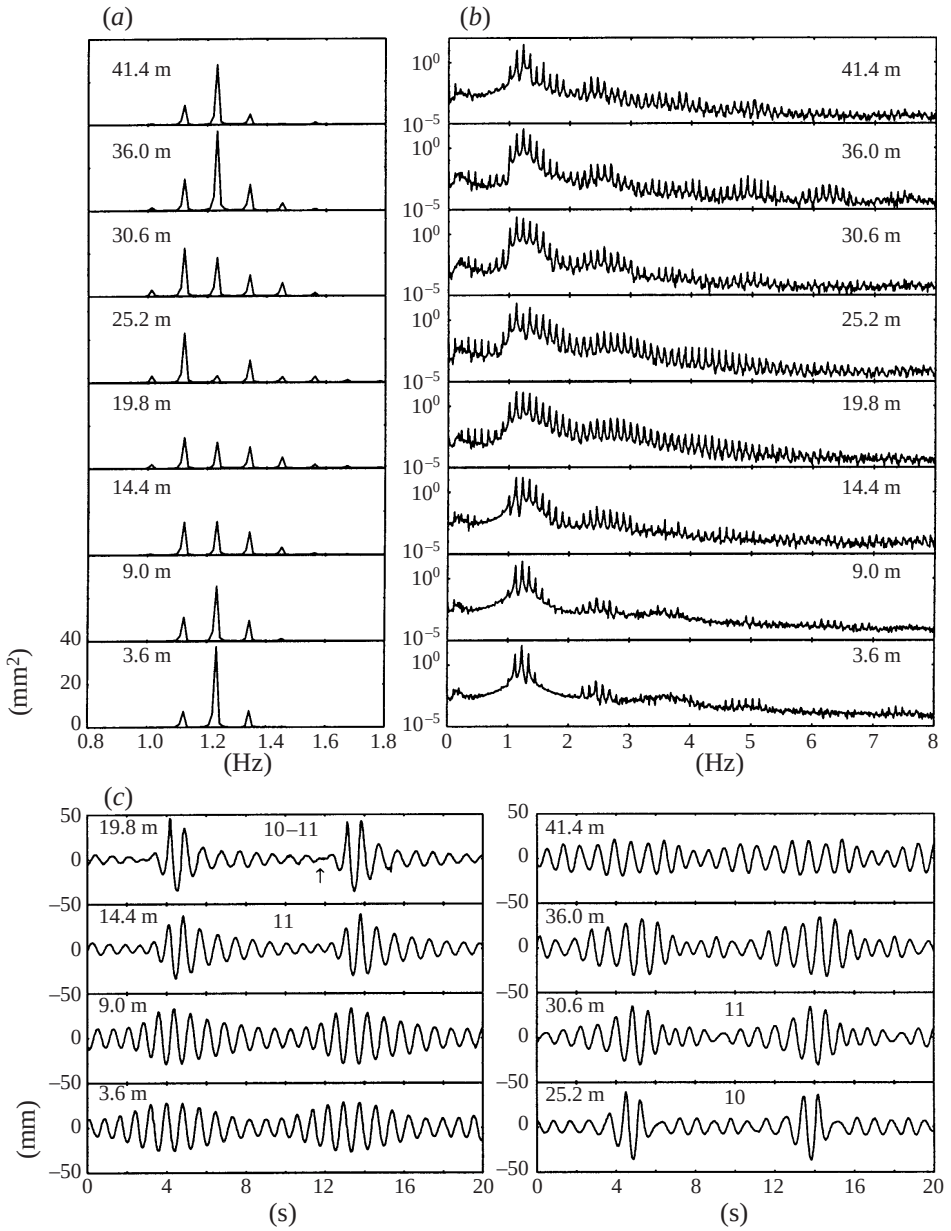

FIGURE 9. (*a*) Linear–linear plot of the spectral evolution with fetch in case of recurrence. $\lambda = 1.0$ m (1.23 Hz), side band frequencies are 1.12 Hz and 1.34 Hz, initial carrier wave steepness is $\epsilon = 0.1$, $\hat{\delta} = 0.894$, and the sideband steepnesses are $b_{\pm}/a_c = 0.3535$. Fetches are 3.6, 9.0, 14.4, 19.8, 25.2, 30.6, 36, and 41.4 m from bottom to top. Frequency resolution of the spectrum is 0.0122 Hz. (*b*) Same as (*a*) but in log-linear scale showing the generation of high-frequency spectral peaks. (*c*) Surface elevation time series showing the evolution of the modulational wave train experiencing a recurrence phenomenon. The time coordinate was shifted in order to follow the same wave group. The numbers 10 and 11 indicates the approximate number of waves per group.

ϵ	$b_{\pm}/a_0$	$\hat{\delta}$
0.12	0.5	0.4 0.5 0.6 0.7 0.8 0.9 1.0
0.13	0.4	0.2 0.3 0.4 0.5 0.6 0.7 0.8 0.9 1.0 1.2
0.165	0.1	0.5 0.55 0.60 0.65 0.7 0.75 0.8 0.85 0.9 0.95 1.0 1.05 1.1
0.165	0.3	0.2 0.4 0.6 0.8 1.0 1.2 1.4
0.165	0.4	0.1 1.3 1.4
0.2	0.15	0.2 0.4 0.6 0.7 0.8 0.9 1.0 1.1 1.2 1.3 1.4 1.5
0.25	0.1	0.2 0.4 0.6 0.7 0.8 0.9 1.0 1.1 1.2 1.3
0.28	0.05	0.43 0.64 0.75 0.86 0.91 0.96 1.02 1.1 1.28

TABLE 2. List of 2.3 m runs conducted.

waves, $\epsilon = 0.133$ and $\hat{\delta} = 0.785$, the initial sideband amplitudes were thereby studied, and at the same time the evolution of this breaking system could be observed over the widest possible range. The second series, see table 2, utilized 2.3 m waves over a wide range of conditions: $\epsilon = 0.12$–0.28; $\hat{\delta} = 0.1$–1.5; various $b_{\pm}/a_0$. These latter experiments allowed an overview of evolution and breaking over the entire map of evolution variables, $\hat{\delta}$ versus ϵ.

4.2.1. *The appearance and regimes of breaking*

In all of the experiments reported here, breaking and its location were observed visually. In certain experiments, breakers for waves of length 1.4 m were photographed (still, standard and high-speed video) breaking in wave groups in the test section of the tank. Deforming and breaking wave shapes were also measured with an array of 16 wave wires. Under breaking conditions, each wave passing through the peak of a wave group invariably broke; however the appearance of the breakers varies, and seems determined both by the phase of the individual wave relative to the wave group peak (as observed in LONGTANK simulations) and by turbulent scars left in the water by previous breakers. The waves do not generally break in a strictly two-dimensional pattern across the tank, cyclical patterns being observed in which alternate breaking occurs at the sides and then at the tank centre, the latter resembling three-dimensional breakers observed in the open ocean, Jessup *et al.* (1997). All of the breakers with wavelengths from 1 to 4 m broke with the formation of a jet at the crest, and more than half of these were energetic, with noticeable jet splash on a decidedly concave front face.

In figure 10, three separate waves are caught breaking by a 35 mm camera, see the caption; these photographs can be related to figure 11 and the discussion below. High-speed camera views of a plunging jet are shown in figure 12.

In breaking at the group peaks, the waves first deform, the front face steepening and becoming increasingly concave and eventually vertical near the crest, which continually sharpens, with the eventual formation of small transverse scallop-like instabilities, the steepening-crest phase, figure 11(*a*). This is followed by the plunging-jet phase, wherein a small jet forms at the crest, figure 11(*b*), grows, figure 11(*c*), and plunges downward until it touches the concave front surface of the wave, figure 11(*d*), at a point generally lower than the crest by not more than 0.40 of the total wave height, depending on the breaker strength. This begins the splashing-ploughing phase, figure 11(*e*), in which the plunging jet, with a severity depending on its strength, enters the water moving forward and downward due to a strong ploughing action,

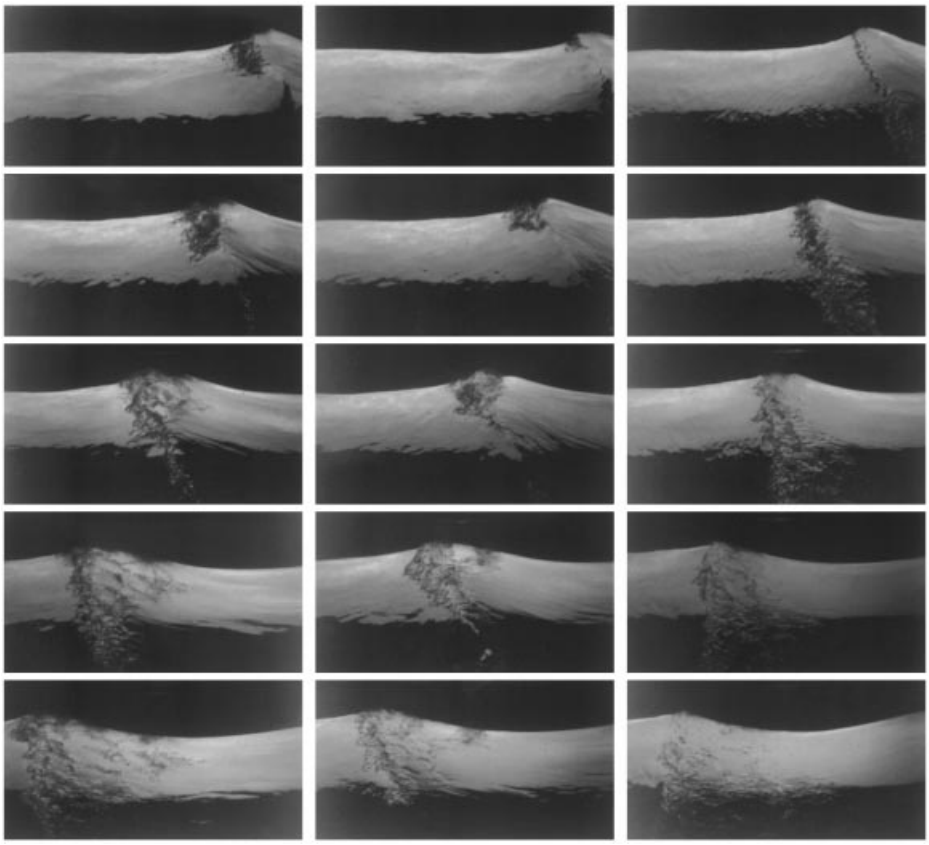

FIGURE 10. Three examples (read each from top to bottom) of 2.3 m waves, initial steepness = 0.165, breaking in wave groups. Each sequence begins with a jet appearing at the crest (top) and ends with a surface scar (bottom), see figure 11. In the sequence on the right, wind is blowing C/U(wind) = 0.32. Water is lit from below, and a vertical board is in the background. Photographed with a 35 mm camera in auto-sequence.

figure 11(*f*). The now submerged jet in this way creates a new front ahead of it, followed by a strongly turbulent region between this new front and the old wave crest, figure 11(*g*). With the subsiding of the active splashing jet and its turbulent underwater structures, a weaker turbulent decaying scar phase ensues in the water, figure 11(*h*), in which the scar moves more and more slowly and less energetically relative to the wave, resulting finally in quietening of the surface and the formation in the ocean of a thin foam layer until another breaking cycle occurs in the vicinity. The appearance of the breaking process is similar for the wavelengths 1–4 m, but as the wavelength increases in this range the visibility of the splashing and foaming process also increases. Some of the waves are noticeably weak, with flatter front faces and weaker jets, which appear to the naked eye as spilling breakers near the wave crest. Incidentally, wind waves with lengths of 60 cm and less have also been observed in the OEL tank. The waves crest and deform, but the jet and subsequent splash are effectively suppressed due to surface tension, presumably, causing the formation of microbreakers, as observed by Melville (1982) for his mechanical waves of 40 cm wavelength.

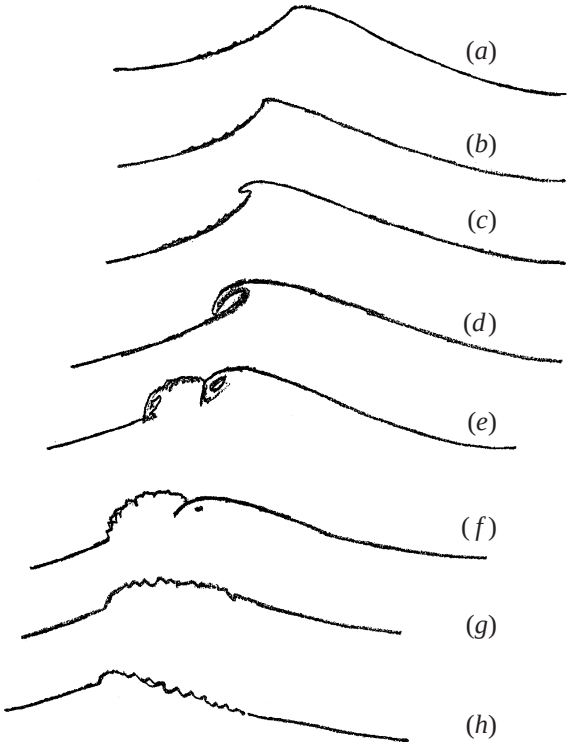

FIGURE 11. Schematics of breaking waves at the group peak, depicting various phases: steepening-crest phase (*a*); plunging-jet phase, (*b*), (*c*), (*d*); splashing-ploughing phase, (*e*), (*f*), (*g*); and decaying scar phase, (*h*).

4.2.2. *The evolution of* 1.2 *m breaking waves*

The emphasis here is on the evolution of the three original waves, and these are shown in figure 13. For cases other than $b_{\pm}/a_0 = 0.03$, the fetches were shifted in the plotting in order to bring the evolution curves into congruence. A single shifting algorithm sufficed: $(kx)_{shift} \equiv \ln\{(b_{\pm}/a_0)/0.03\}/\beta$, where β is the initial growth rate. The horizontal bar indicates the location of breaking. General characteristics such as exponential growth, asymmetry of the upper and lower sidebands near the maximum modulation, and permanent downshifting after breaking, are seen not to be altered by the initial sideband amplitude $b_{\pm}/a_0$. This result is very reassuring for interpretation of experiments. A moderate scatter of the data points is seen near the breaking region, as might be expected.

The steepness of these waves, $\epsilon = 0.133$, is close to values typical of the ocean, and the breaking is reasonably vigorous. They therefore serve well as a prototype breaking system and demonstrate most of the characteristics seen first by Melville for shorter and steeper waves, notably the effect of breaking to increase the asymmetry, $(b_- - b_+)$, and to render it irreversible. We discuss this in greater detail later (§ 5) and meantime pay attention to the end state of the evolution as it was measured. The energy originally residing largely in the carrier wave is now divided roughly between two waves, the original carrier and the lower sideband. The future evolution of this two-wave system, which it was impossible to measure here for lack of fetch, can be expected to be different from that of the Benjamin–Feir three-wave systems studied here.

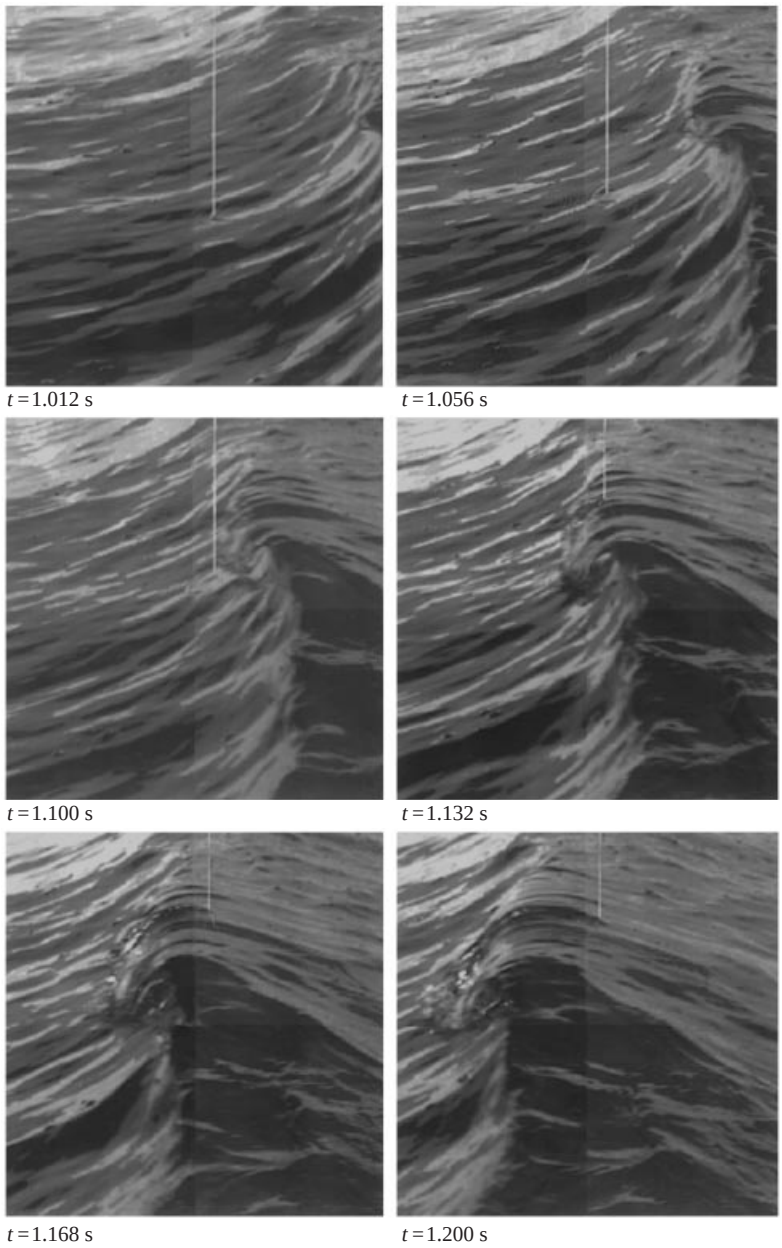

FIGURE 12. High-speed camera images of a plunging jet during wave breaking. The vertical line is a fixed string at the centre of the tank. $\lambda = 2.3$ m, $T = 1.2$ s, $ak = 0.165$.

4.2.3. *The evolution of* 2.3 *m waves*

Among all 2.3 m cases, table 2, certain conditions are selected for discussion in figure 14 showing the evolution of wave modes with fetch. The cross-hatched part indicates the region in fetch where a series of breakers was observed, and the solid line is a curve-fitted exponential growth. The symbols represent the normalized amplitude of the carrier, the lower and the upper sideband modes.

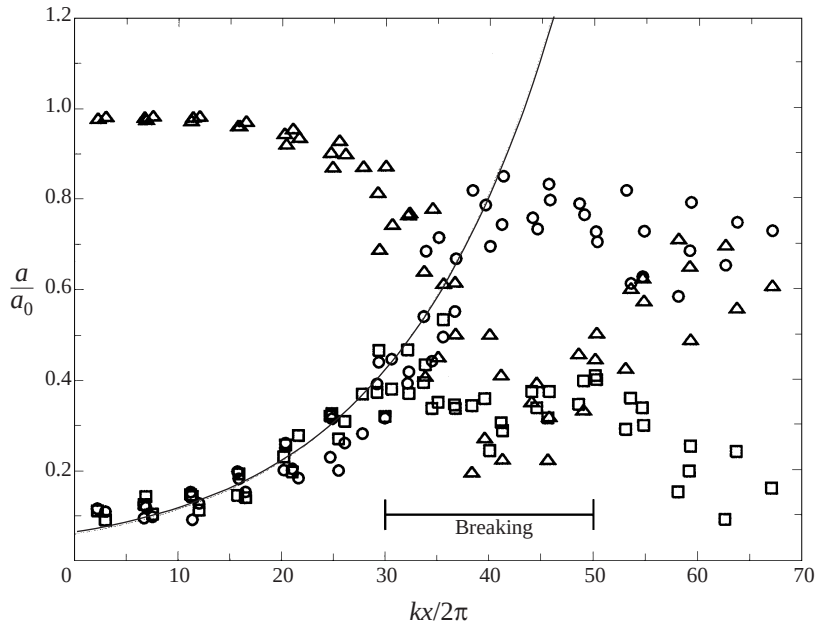

FIGURE 13. Breaking prototype: 1.2 m, 1.14 Hz, 1.029 Hz, 1.267 Hz, $\epsilon = 0.133$, $\hat{\delta} = 0.785$, and b_+/a_0 3 % to 50 %. Symbols are: ○, lower sideband; □, upper sideband; △, carrier sideband.

Figure 14(*a*) displays the evolution of 2.3 m, $\epsilon = 0.165$ waves with $\hat{\delta} = 0.6$, 0.8 and 1.0. The initial sideband amplitudes $b_\pm/a_0$ were set at a constant value of 0.1 for all cases. The onset of breaking indicated by a vertical line is closest to the wavemaker around $\hat{\delta} \sim 0.8$. This may indicate a maximum growth of the sideband. For all cases, at near peak modulation, the lower sideband amplitude exceeds the upper sideband amplitude. However, the amplitudes of the upper and the lower sidebands start to deviate earlier than the onset of the breaking. This differs with Melville (1982) where the breaking was seen prior to the onset of the asymmetric development of the sidebands. The asymmetric development of sidebands was also seen earlier for the recurrence case without breaking, § 4.1.

In figure 14(*c*), the evolution of 2.3 m, $\epsilon = 0.28$ wave with $\hat{\delta} = 0.43$, 0.64, 0.86 and 1.1 are presented. The initial sideband amplitudes $b_\pm/a_0$ were set at a constant value of 0.05 for all cases. Contrary to the $\epsilon = 0.165$ case, the onset of breaking is earlier here than the onset of asymmetric development of the sidebands. The case $\hat{\delta} = 1.1$ (lower right figure) had only a single weak breaker, but still experienced an asymmetric growth of the sidebands.

From these observations, we may conclude that the asymmetric growth of the sidebands does not absolutely require the appearance of breaking. We show later that it can be initiated by spreading of discretized energy to higher frequencies, as well as by breaking. Previous studies have also shown that asymmetry can appear in the absence of dissipation (Lo & Mei 1985; Dommermuth & Yue 1987; Trulsen & Dysthe 1990; Hara & Mei 1991).

For both $\epsilon = 0.165$, $b_\pm/a_0 = 0.1$ and $\epsilon = 0.28$, $b_\pm/a_0 = 0.05$, in figure 14, the waves continued breaking until reaching the end of the tank. In order to study the evolution beyond the point where breaking ceased, we have conducted an experiment with higher initial sideband amplitudes, figure 14(*b*); 2.3 m, $\epsilon = 0.165$, $\hat{\delta} = 0.2$–1.4,

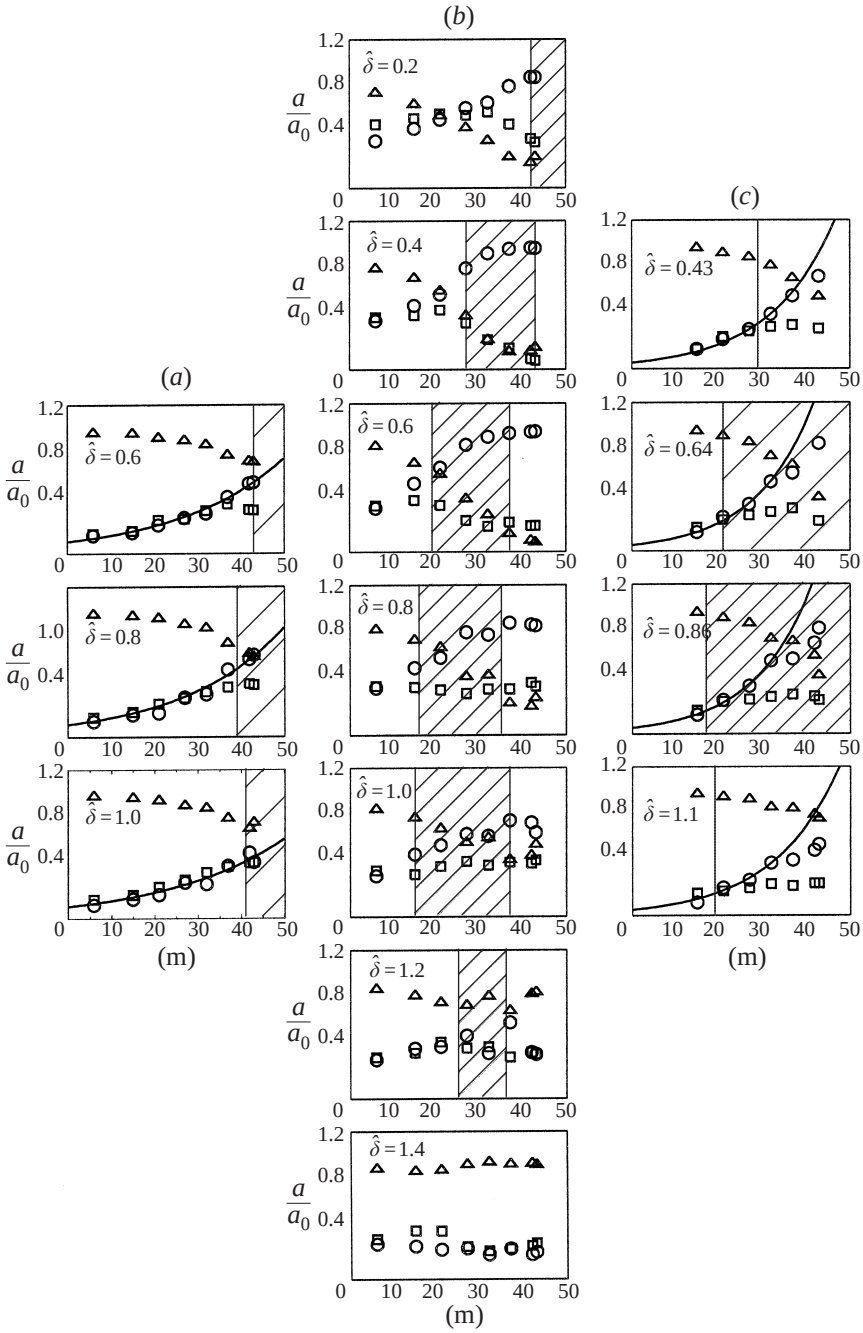

FIGURE 14. Evolution of wave modes for 2.3 m wave: (*a*) $\epsilon = 0.165$, for $\hat{\delta} = 0.6$, 0.8 and 1.0, $b_{\pm}/a_0 = 0.1$; (*b*) $\epsilon = 0.165$, $\hat{\delta} = 0.2$, 0.4, 0.6, 0.8, 1.0, 1.2, and 1.4, $b_{\pm}/a_0 = 0.3$; (*c*) $\epsilon = 0.28$, $\hat{\delta} = 0.43$, 0.64, 0.86 and 1.1, $b_{\pm}/a_0 = 0.05$. Shaded part indicates where the waves broke. Symbols are: △, carrier; ○, lower; □, upper.

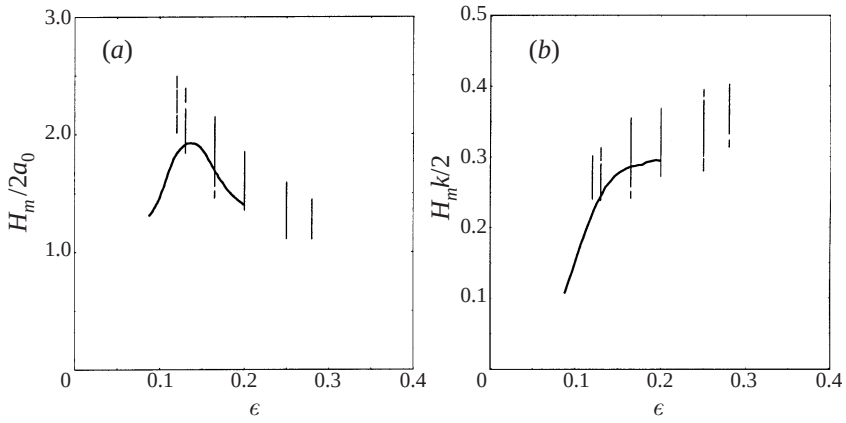

FIGURE 15. (*a*) Ratio of the maximum amplitude $H_m/2$ of waves to the initial amplitude a_0, as a function of ϵ. (*b*) The maximum wave steepness $H_mk/2$ versus the initial steepness ϵ. Vertical lines show the current study, while the curves are from Su & Green (1985).

$b_{\pm}/a_0 = 0.30$. The breaking ceases for $\hat{\delta} = 0.4$, 0.6, 0.8, 1.0 and 1.2, and except in the last case, a permanent downshifting occurs. Compare this result with the evolution presented earlier in figure 13, where the carrier wave eventually recovers its amplitude, and there seems to be an exchange of energy between the lower and the carrier wave mode whereas the upper sideband wave remains small in amplitude. In figure 14(*b*), we see only a slight indication that the carrier wave has started to regain its energy. Note that for $\hat{\delta} = 1.2$, downshifting was not completed despite breaking, showing the dependence of the final state on the strength of breaking.

4.2.4. *High-frequency spreading*

The spreading of energy at higher frequencies is noticeable during evolution and occurs both with (figure 20: $\hat{\delta} = 0.785$) and without (figure 9: $\hat{\delta} = 0.894$) breaking. The spread energy is decidedly discretized and there is little evidence of the presence of a continuous spectrum underlying it. In the case of 2.3 m waves with very small sideband spacing, $\hat{\delta} = 0.2$ (figure 22), both discretized and continuous energy are evident, the latter growing with fetch and especially prominent just to the high-frequency side of the peak. The spectral resolution in the latter case is just sufficient to see the discrete peaks, and the appearance of what looks like a continuous spectral component is considered to be real.

4.2.5. *Characteristics of breaking on* 2.3 *m waves*

Following Su & Green (1985), the measured steepness $H_mk/2$ where H_m is the total wave height at breaking, is shown for various initial wave steepnesses ϵ. The ratio of $H_m/2a_0$, is plotted as well (figure 15); note that $H_m/2$ is not the wave amplitude at breaking as the crest height there significantly exceeds the trough amplitudes. There are slight differences at the lower steepness, but the general tendencies at the higher steepnesses are similar to each other. Note that in Su & Green's experiments, $\delta\omega$ is not fixed or varied, but is determined naturally. On the other hand, our results contain a larger range of modulational frequencies, and there is, therefore, a wider scatter of $H_m/2a_0$ and $H_mk/2$. In addition, even for the same initial steepness and modulational frequency, each breaking wave has a different $H_mk/2$, introducing natural scatter, in part due to the effect of disturbances left in the water by previous breakers.

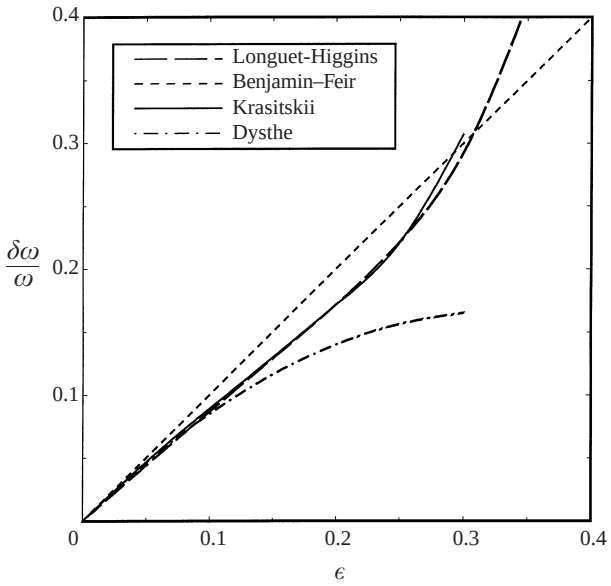

FIGURE 16. The $(\epsilon, \delta\omega/\omega)$ diagram, indicating the theoretical prediction of the locus of the maximum growth.

4.2.6. *The regime of breaking; the minimum steepness for breaking*

The fastest growing instability occupies a corridor in ϵ, $\hat{\delta}$. Theoretical predictions are shown in figure 16 of the most unstable modulational frequency, $\delta\omega/\omega$, as a function of initial wave steepness ϵ, according to Benjamin & Feir (1967), Dysthe (1979), Longuet-Higgins (1980) and our own calculations, previously unreported, based on the kinetic equations of Krasitskii (1994). For each steepness $\epsilon = 0.13$, 0.165, 0.2, 0.25 and 0.28 seeded experiments were conducted with modulational frequencies in the range from $0.1 \leqslant \hat{\delta} \leqslant 1.5$. The thick vertical lines in figure 17 indicate the range of modulational frequencies where the location of breaking inception in the tank was closest to the wavemaker. This roughly coincides with the almost identical theoretical predictions of Longuet-Higgins (1980) and Krasitskii (1994), tending to confirm them. Note that Dysthe's (1979) theoretical prediction of the most unstable frequencies are in agreement with these only for steepness $\epsilon < 0.10$.

Breaking occurs only in a bounded portion of ϵ, $\hat{\delta}$, and it is interesting to know the boundaries, particularly for small steepness. Su & Green (1985) showed experimental curves extending to steepness, ϵ, a little smaller than 0.11. In LONGTANK, which was not extended much beyond the first peak in the modulational cycle, breaking was not found for $\epsilon < 0.13$. Figure 17 shows the experimental boundaries for breaking as determined in these experiments; steepness smaller than $\epsilon = 0.12$ could not be investigated because of tank length limitations. It can be seen, however, that the extrapolated boundary intersects the most unstable corridor for steepness slightly larger than 0.10. We have supplemented our experimental observation with numerical (fully nonlinear) breaking results, Landrini *et al.* (1998). Although more calculations would be useful, a minimum steepness ϵ for breaking just below 0.1 seems indicated. It should be noted that the steepness, ϵ, corresponds to the average energy within the energetic wave train and not that of the wave at the modulation peak, which is substantially larger, as indicated in figure 15.

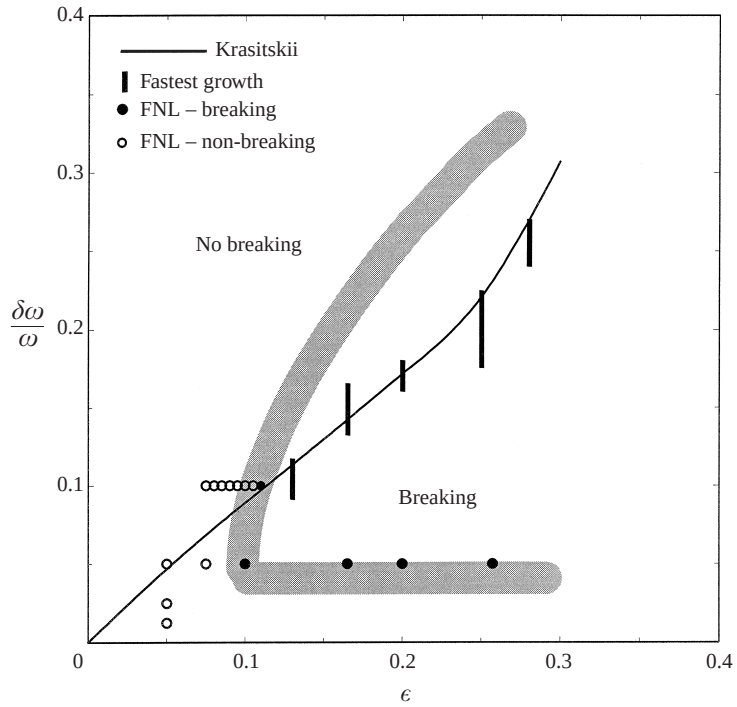

FIGURE 17. The $(\epsilon, \delta\omega/\omega)$ diagram, displaying the region where breaking events were observed. Circles are from fully nonlinear computations of Landrini *et al.* (1998). Thick grey line indicates an approximate breaking–non-breaking boundary as determined from the experiment.

Since energetic wave steepnesses in the ocean are in the vicinity $\epsilon \sim 0.10$, an important region of modulational frequencies, $\hat{\delta}$, for the ocean consistent with figure 17 is $0.05 < \hat{\delta} < 0.10$.

5. Discussion

5.1. *Downshifting during recurrence*

Theoretical evidence of perfect recurrence found through NLS simulations has been supported by three-wave calculations by Stiassnie & Shemer (1987) using Zakharov equations. In their case, a common characteristic of the predicted dynamical behaviour during strong growth of the sidebands is that the difference in energy between them is notable; they predicted that at peak modulation the upper sideband amplitude becomes greater than that of the lower; however the NLS simulations predict that initially identical sideband amplitudes remain identical throughout the motion.

The experimental evidence contradicts this prediction. In Lake *et al.*, a growth of the lower sideband relative to the upper was found during their mutual growth, both with and without breaking, and we have found the same here. The spectral asymmetry created in this way has been predicted by computations made by the Dysthe modification of the NLS idealization (Lo & Mei 1985; Trulsen & Dysthe 1990; Hara & Mei 1991), which results in an improvement at finite bandwidths; the same prediction was also made by Dommermuth & Yue (1987) using exact numerical calculations by a spectral method.

Experiments show that a further consequence of three-wave modulation, breaking

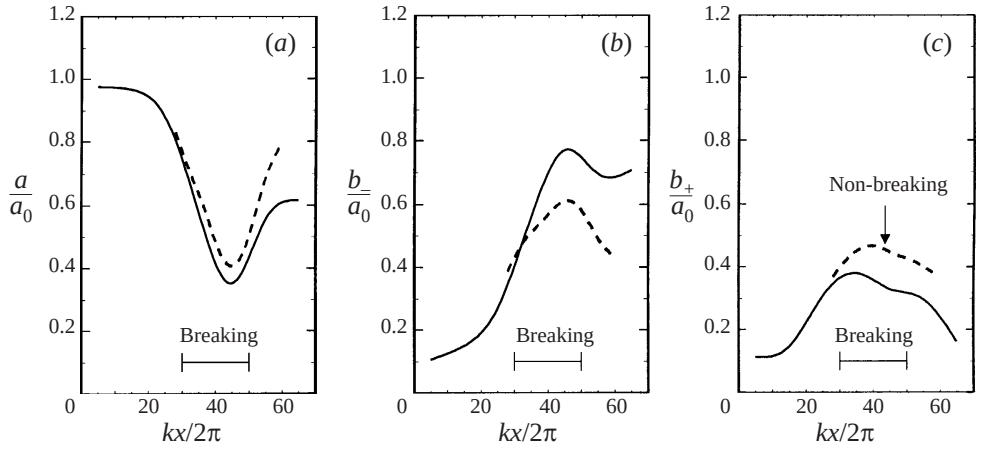

FIGURE 18. Evolution of the wave modes for cases with and without breaking events: (*a*) the carrier, (*b*) the lower and (*c*) the upper sideband waves are presented. The solid line is the evolution of the case with breaking, and the broken line is the evolution of the non-breaking case. Breaking case is $\epsilon = 0.133$, $\hat{\delta} = 0.785$: non-breaking case is $\epsilon = 0.1$, $\hat{\delta} = 0.894$.

or not, is the appearance of discretized energy in the spectrum at frequencies higher than $\omega_+ + \delta\omega$. As we discuss below, the asymmetry, $(b_- - b_+) > 0$, would seem an inevitable consequence of the existence of this high-frequency energy.

In the absence of breaking, can perfect recurrence ultimately occur in the face of this discretized high-frequency energy and the resulting sideband asymmetry? It seems unlikely, and fully nonlinear calculations of Landrini *et al.* (1998) show deviations from perfect recurrence from cycle to cycle, and particularly in the breaking cycle. In the experiment here, however, the tendency toward reversal of the lower–upper imbalance and toward recurrence is found to be quite strong for a wave train sufficiently weak that breaking is absent. The emphasis here is on 'tendency'. From the point of view of conservative system theory, further attention should be devoted to the discretized high-frequency energy, its causes and consequences.

5.2. *Downshifting during breaking*

In previous sections, we have shown the evolution of the modulational wave train with a variety of parameter ranges. One showed recurrence, others showed permanent downshifting of the spectral peak. Figure 18 summarizes the evolution of wave modes for cases with and without a breaking event, which were presented earlier in figure 13 and figure 9; from left to right, the carrier, the lower, and the upper sideband evolutions are presented. The solid line is a smoothed curve of the evolution of the breaking case ($\epsilon = 0.133$, $\delta\omega/\omega = 0.104$, and $\hat{\delta} = 0.785$), and the broken line is a smoothed curve of the evolution without breaking ($\epsilon = 0.1$, $\delta\omega/\omega = 0.089$, and $\hat{\delta} = 0.89$). A horizontal bar in each diagram represents the approximate location of the breaking event for the breaking case. Due mainly to differences in steepness, the time scale associated with evolution is different for each case. Therefore, in order to illustrate the difference in the evolution in a single diagram, the horizontal coordinate of the non-breaking case was artificially adjusted; it was offset by 25 wavelengths, and was shrunk by a factor of 0.83.

A notable difference between the two cases is that the lower sideband remains high in amplitude when and after breaking, whereas when no breaking is present it

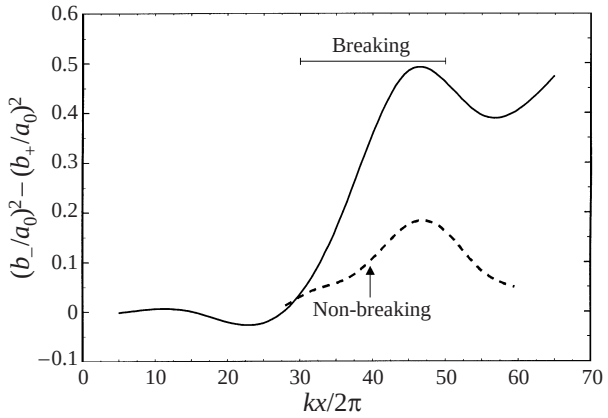

FIGURE 19. The evolution of the energy difference of the lower and the upper sideband modes. The solid line is the breaking case, and the broken line is the recurrence case.

subsides after peaking. On the other hand, the upper sideband seems to return to its original state in both cases. Therefore, the energy difference of the lower sideband and the upper sideband remains large when breaking is present but returns to zero when no breaking is present. This is illustrated in figure 19, where the difference of the square of the amplitudes of the lower and the upper sideband is plotted against non-dimensional fetch. It is clear that the effect of breaking dissipation is to increase and render irreversible the energy difference of the upper and the lower sideband after peak modulation. The spectral evolution of the breaking case is shown for 10 wave length separations in figure 20. The spectral downshifting is clearly seen, in the linear spectral energy plot, figure 20(*a*). Below we will present a physical interpretation of such spectral behaviour based on global considerations including energy and momentum losses in the wave system, already introduced in § 2.

5.3. *Downshifting theory*

Here we present an analysis of energy shifting in a system of discrete waves, extending the results of Tulin (1996). Our purpose is simple: to predict based on global considerations of wave energy and momentum, the consequences for energy shifting of (i) both energy dissipation, D_b, and momentum loss, $\dot{M}_b$, due to breaking, and (ii) the transfer of energy in the discretized spectrum.

Consider a system of planar waves in which the free wave energy is initially distributed in three waves: primarily in a carrier wave, ω_0, and to a lesser extent in two sidebands, $\omega_0 \pm \delta\omega$. The initial energy in this three-wave system is

$$E_3 = E_0 + E_{-1} + E_{+1} + \sum_j E_j, \tag{5.1}$$

where E_0, E_{-1}, E_{+1} are the energies in the first harmonics of each of the three waves and $\sum_j E_j$ represents the energy arising from the interactions between three fundamentals, comprising the energy in the bound harmonics which arise from self-interactions, and the energy in the sum and difference harmonics which arise from inter-wave interactions.

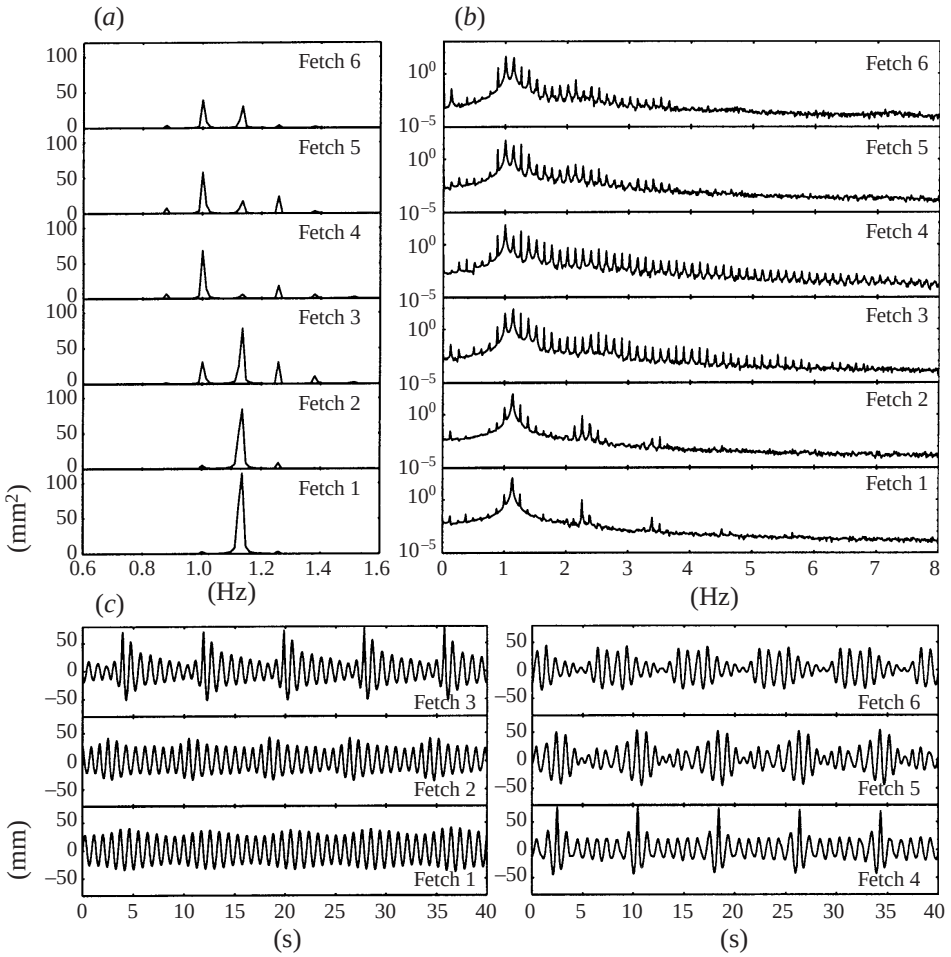

FIGURE 20. Spectral evolution of breaking wave case: wavelength 1.2 m, frequencies 1.14 Hz, 1.029 Hz, 1.267 Hz, $\epsilon = 0.133$, and $\hat{\delta} = 0.785$. Spectrum is plotted for every 10 wavelengths, sampled from the data presented earlier in figure 13 as the breaking prototype.

In a similar way, the initial momenta in the three wave system are

$$M_3 = M_0 + M_{-1} + M_{+1} + \sum_j M_j. \tag{5.2}$$

The initial distribution of energy and momenta, (5.1) and (5.2), is altered by the transfer of energy to free waves $\omega_0 \pm n\delta\omega$, first most noticeably to $n = +2$, then $n = -2, +3$, etc. These relatively fast transfers seems to be a consequence of detuned resonances of which the first is

$$\left.\begin{aligned}(\omega_0) \mp (\omega_0 - \delta\omega) \pm (\omega_0 + \delta\omega) &= \omega_0 \pm 2\delta\omega,\\ (k_0) \mp (k_0 - \delta k) \pm (k_0 + \delta k) &= k_0 \pm 2\delta k + \Delta k,\end{aligned}\right\} \tag{5.3}$$

in which Δk is a small detuning factor, where $\Delta k/k$ is $O(2(\delta\omega/\omega)^2)$, allowing effective energy exchange over a distance comparable to $(2(\delta\omega/\omega)^2)^{-1}\lambda$, where λ is the wavelength.

In the experiments, see figure 9(*b*), the early growth of $\omega_0 + 2\delta\omega$ can be seen even

at 3.6 m fetch and followed until it returns its energy in recurrence after 30.6 m or after about 30 wavelengths. The subsequent growth of $\omega_0 + 3\delta\omega$ and even higher free waves can also be seen. The growth of $\omega_0 - 2\delta\omega$ appears at 9.0 m, continuing until it too begins to recede after 30.6 m. For reasons not yet understood, the growth of high-frequency free waves through resonant interaction outstrips the growth of low-frequency free waves and especially beyond $\omega_0 - 2\delta\omega$.

The growth of these new free waves must occur at the expense of the three-wave system, E_3. If, at the same time we presume that breaking is taking place, then

$$\dot{E}_3 = -D_b - \sum_{n=\pm 2, \pm 3, \ldots} \dot{E}_n, \tag{5.4}$$

and, likewise,

$$\dot{M}_3 = -\dot{M}_b - \sum_{n=\pm 2, \pm 3, \ldots} \dot{M}_n. \tag{5.5}$$

The momentum in each wave component, both free and bound, can be shown to be given to second order in wave steepness (ϵ) by

$$M = E/c = E/(\omega/k), \tag{5.6}$$

and then, utilizing $\delta k/k = 2\delta\omega/\omega$, and neglecting terms of $O(\delta\omega/\omega)^2$, the three-wave momentum, M_3, becomes

$$c_0 M_3 = E_0 + E_{-1}(1 - \delta\omega/\omega) + E_{+1}(1 + \delta\omega/\omega) + \sum_j (c_0/c_j) E_j, \tag{5.7}$$

and subtracting the above from the three-wave energy, E_3, (5.1):

$$E_3 - c_0 M_3 = (\delta\omega/\omega)(E_{-1} - E_{+1}) + \sum_j E_j (1 - c_0/c_j). \tag{5.8}$$

Taking the time derivative of (5.8) and subtracting (5.4) and (5.5), finally the time variation of the difference between the lower and upper sideband energies is obtained with the dependence originally sought:

$$\frac{\partial}{\partial t}(E_{-1} - E_{+1}) = \underbrace{-(D_b - c_0 \dot{M}_b)/(\delta\omega/\omega)}_{\text{(i) breaking}} + \underbrace{\sum_{n=\pm 2, \cdots} \dot{E}_n \left(\frac{\omega_n - \omega_0}{\omega_0}\right) \Big/ (\delta\omega/\omega)}_{\text{(ii) energy transfer to free waves}} + \underbrace{\sum_j \dot{E}_j \left(\frac{c_0 - c_j}{c_j}\right) \Big/ (\delta\omega/\omega)}_{\text{(iii) energy in bound waves}}. \tag{5.9}$$

The sum interaction in terms included in (iii) can be seen in experiments arrayed in clusters centred on each harmonic. The growth of these at the second harmonic becomes apparent at 14.4 m fetch, figure 9(*b*), corresponding to growth of the sidebands resulting in stronger inter-wave interactions among the three dominant waves. With growth in other free waves, particularly for frequencies on the high side, the interaction terms grow to the right of the second harmonic. The celerity, c_j, of the interaction waves is c_0 for all harmonics, and somewhat greater or lesser for sum inter-wave interactions, depending on the case. The symmetry of the cluster about the second harmonic tends to minimize the entire contribution, which is already certainly lower than (ii) because of the low levels of interaction energy; the effect of sum interactions can therefore be safely ignored. The energy in difference frequencies is also seen to be small and can be ignored, too, on that account.

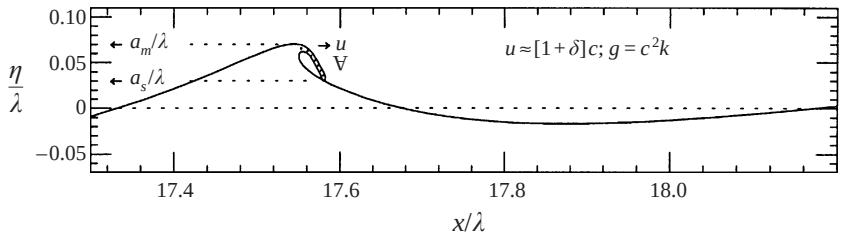

$$\delta E = -\sum\left[\frac{\rho u^2}{2} + \rho g(a_m - a_s)\right]\forall = -\sum[1 + 2\delta + 2(a_m - a_s)k]\frac{\rho c^2}{2}\forall,$$

$$\delta M = -\sum \rho u \forall = -\sum \rho c(1+\delta)\forall = (1+\gamma)\frac{\delta E}{c},$$

where
$$\gamma = \frac{1 - 2a_m k(1 - a_s/a_m)}{1 + 2\delta + 2a_m k(1 - a_s/a_m)} \approx 0.4 \text{ (strong) to } 0.7 \text{ (weak)},$$

$$[\delta \leqslant 0.1; \quad ka_m \approx 0.25 - 0.50; \quad a_s/a_m \approx 0.5 \text{ (strong) to } 0.9 \text{ (weak)}].$$

FIGURE 21. Schematic of breaking wave and jet, with quantification of energy and momentum losses.

Over the duration of our experiments, the important new free waves correspond to -2, $+2$, $+3$, and even $+4$ at the maximum downshift, between fetches 19.8 m and 25.2 m, figure 9(*a*); the low-frequency energy in -2 generally lagged behind the upper high-frequency waves except at the end of the cycle, after recurrence. These facts combine in (ii) to create a positive downshifting contribution from (ii) during the first half of the evolution, explaining the positive sign of $(E_{-1} - E_{+1})$ at midfetch, and its variation throughout, see figure 19, eventually toward recurrence.

The term (ii) in the present theory also explains the necessity to include more than three free waves in a prediction of wave evolution if details such as the variation $(E_{-1} - E_{+1})$ are to be predicted.

The experiments show that when breaking ensues during evolution, then $(E_{-1} - E_{+1})$ grows more rapidly and maintains its positive value at the end of the cycle, figure 19. This can be explained through (i) in (5.9), provided that this term is positive in nature.

During breaking of energetic waves, a jet forms which conveys water with both kinetic and potential energy out of the wave, as well as momentum. This is depicted in figure 21, taken from Tulin (1996), where these losses are quantified and term (i) is parameterized in terms of the breaking dissipation and found to be positive:

$$\frac{\partial}{\partial t}(E_{-1} - E_{+1}) = \underbrace{\gamma D_b/(\delta\omega/\omega)}_{\text{(i)}} + \underbrace{\sum_{n=\pm 2,\ldots} \dot{E}_n \left(\frac{\omega_n - \omega_0}{\omega_0}\right) \Big/ (\delta\omega/\omega_0)}_{\text{(ii)}}, \tag{5.10}$$

where (iii) has been neglected.

The present experiments, summarized in figures 18–20, substantially confirm (5.10). The influence of (ii) which is dependent on ± 2, is negligible since the energy in these waves is small at the end of the breaking cycle. An experimental estimate of $\gamma = 0.4$, in agreement with the theoretical estimate for a strong breaker, figure 21, follows from the data, figures 18 and 19: $\delta\omega/\omega = 0.10$; dissipation loss in E_3 over the breaking event, $0.11E_0$; a concurrent change in $E_{-1} - E_{+1}$ of $0.45E_0$.

The result (5.10) can, in principle, be applied to each cycle of the breaking process,

replacing the set $-1, 0, +1$ by $-2, -1, 0$, leading eventually to another downshifting, $(E_{-2} - E_0) > 0$, provided that breaking takes place. The continuation of the process requires the generation of successive lower sidebands $-2, -3$, etc., but this seems guaranteed by successive near-neighbour detuned resonances, exemplified by (5.3).

The global result, (5.10), leads immediately to a variety of questions: what is the precise mechanism through which breaking brings about the sideband differences leading to downshifting?; what is the effect of wind, which provides both energy and momentum to the waves?; how can (5.10) be translated to a predictive evolution theory in both space and time? The first of these three questions dependent as it is on the breaking process, remains unanswered. The second is answered in Tulin (1996), where it was shown that the wind pumping, $\dot{e}_w$, is essentially equal to cf_w, where f_w is the wind thrust on the wave, so that the wind does not contribute noticeably to downshifting, which depends on the difference between these quantities. In the same reference, a set of heuristic coupled equations was derived for the simultaneous evolution of a narrow banded system in the presence of wind pumping and breaking, one for the peak energy density, and the other, a downshifting equation, for the corresponding group velocity. These equations, or something like them, can be formally derived, but their detailed discussion is beyond the scope of the present work.

Finally, a serious challenge is imposed by these results to any predictive method of ocean wave evolution in which downshifting depends solely on slow, high-order, resonant wave interactions. Just as in the simple case of three-wave evolution treated here, the effect of the imbalance between energy and momentum losses, hand in hand with near-neighbour detuned resonances, both occurring in the order of 50 wavelengths, might very well dominate the downshifting of energetic waves in the ocean, too.

5.4. *Discretized high-frequency spectra*

Melville, who utilized wave steepnesses in the range 0.2–0.3, has given an interpretation of the generation of discretized higher frequencies in terms of the instability of steep waves as quantified by Longuet-Higgins (1978). We found in our experiment noticeable discretized high-frequency energy for steepnesses well below $\epsilon = 0.2$. We draw attention to the log-linear spectra for our prototype breaking wave with an initial steepness 0.133, in figure 20. Even taking into account the increase in the steepness of this wave when breaking is initiated, it would seem to be under 0.3 and less steep than required for the instability described by Longuet-Higgins (1978). Furthermore, the spread of discretized high-frequency energy was very vigorous during the strong modulation of the weak three-wave system, $\epsilon = 0.1$, where a tendency to recurrence was observed and where no breaking occurred, see figure 9. These facts, plus the way in which the energy spreads, makes it highly likely that high-frequency discretized energy spreading has its origin elsewhere than in steep wave instability.

As described in some detail in § 5.3, the spread of discretized energy around the initial three-wave system, which occurs over about 30 wavelengths, seems a likely consequence of the near-neighbour detuned resonance described by (5.3); at the same time, the spread of discretized energy around the harmonics of the three-wave system seems first of all due to self- and wave-wave interactions associated with the three free waves. However, it should not be overlooked that energy may also be spread in the harmonic clusters into neighbouring bound waves, through the detuned resonance

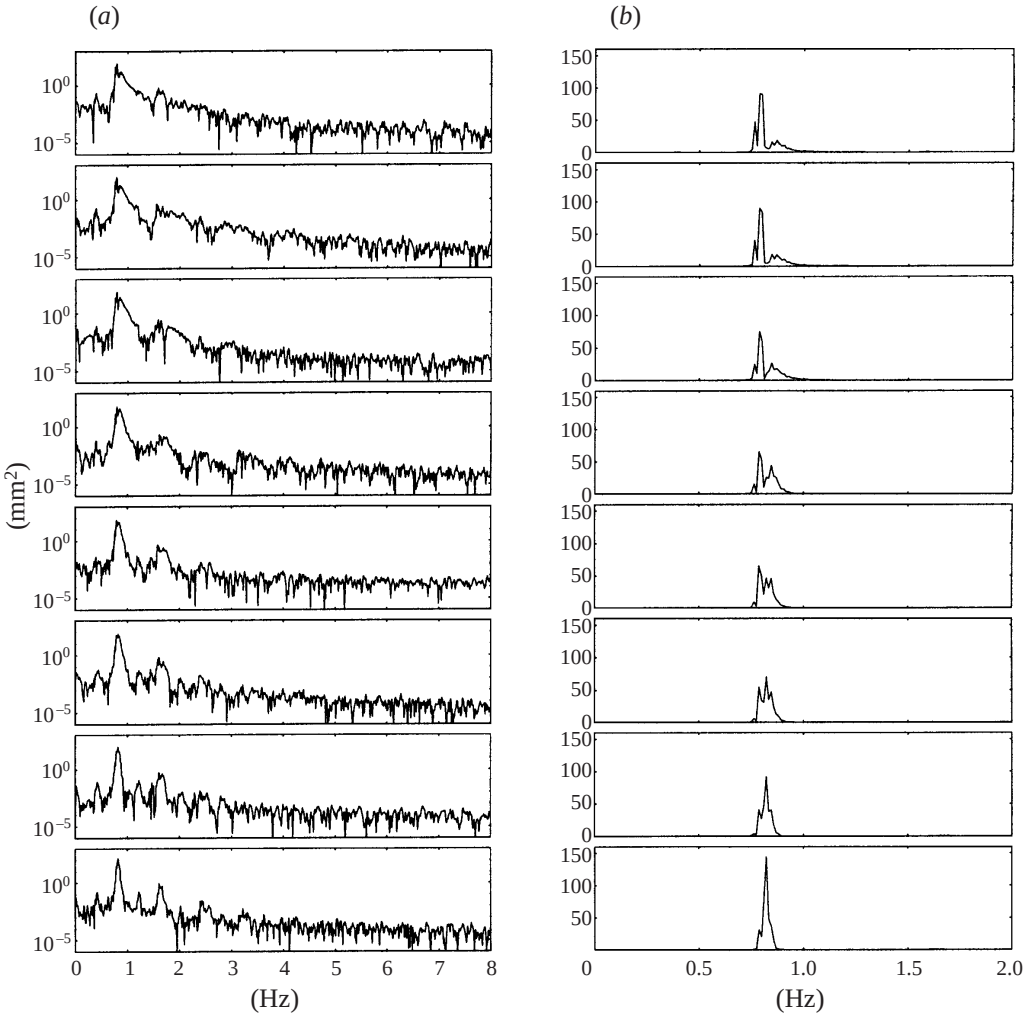

FIGURE 22. Spectral evolution of wavelength 2.3 m, 0.825 Hz, $\epsilon = 0.165$, $\hat{\delta} = 0.2$, and $b_{\pm}/a_0 = 0.3$. Frequency resolution of the spectrum, 0.012 Hz, is marginal but still sufficient to resolve the sideband and the carrier wave separation of 0.027 Hz in the linear-linear plot (*b*).

involving three generating bound waves, of which the first example is

$$\left.\begin{aligned}(2\omega_0) \mp (2\omega_0 - \delta\omega) \pm (2\omega_0 + \delta\omega) &= 2\omega_0 \pm 2\delta\omega,\\ (2k_0) \mp (2k_0 - \delta k) \pm (2k_0 + \delta k) &= 2k_0 \pm 2\delta k + \Delta k,\end{aligned}\right\} \tag{5.11}$$

where again $\Delta k/k$ is $O(2(\delta\omega/\omega)^2)$ and these interactions too are observed in experiments to occur within 30 wavelengths. This detuned resonance of bound waves may be compared with the free wave case, (5.3).

5.5. *Continuous spectra*

The spectra appearing after breaking in Melville are characterized by the appearance of a substantial continuous spectrum underlying the discrete; see Melville (1982) figure 7 for $\epsilon = 0.233$, and figure 9 for $\epsilon = 0.292$. In our experiments we do not see significant signs of a continuous spectrum for evolution at normal sideband spacings

and for $\epsilon = 0.1$ (figure 9) and for $\epsilon = 0.133$ (figure 20). We did find substantial continuous spectra on the high side of the spectral peak at a very small sideband spacing, $\hat{\delta} = 0.2$ (figure 22). These contrasting results suggest that both wave steepness and sideband spacing are important factors with regard to mechanisms whereby continuous spectra are created and become observable. In addition, the separation of discrete and continuous spectra depends on the frequency resolution realized in the data processing, which is itself the inverse of data length.

Randomized fluctuations in wave frequency imposed on discrete waves would if sufficiently large lead to the appearance of a continuous spectrum; a sufficiently large fluctuation intensity would be of the order $\delta\omega$. Breaking waves leave behind them patches or scars of turbulence and enhanced surface drift in the down-tank direction. These would lead, at least, to fluctuations (increases) in the apparent wave frequency due to Doppler effects. These fluctuations would, of course, be larger for steeper waves; here it is important to remember that the breaking dissipation grows non-linearly with wave steepness. The effect of given fluctuations would also be greater for smaller $\hat{\delta}$. These remarks, taken together with the previous experimental observations, suggests the necessity for further observation including wind effects if possible, and for quantification of the effects involved.

5.6. *Wave crest change*

Wavenumber downshifting implies by definition a reduction of wave crest density, $(N/\Delta x)$, where $N = (\Delta x)(k/2\pi)$ is the number of wave crests in an interval Δx. It then follows that the rate of change in wave crest density is identically equal to the frequency down-shifting rate following a group. The wave conservation law is

$$\partial k/\partial t + \partial(ck)/\partial x = 2\pi(\dot{N}/\Delta x), \tag{5.12}$$

where (ck) is the flux of wave crests. This leads to the desired relation

$$\partial\omega/\partial t + c_g\partial\omega/\partial x = (\mathrm{d}\omega/\mathrm{d}t)_{c_g} = 2\pi c_g(\dot{N}/\Delta x). \tag{5.13}$$

The latter is a kinematical identity and does not imply in any way that crest number change is the causative effect leading to frequency downshifting. Rather, they are alternative measures of the same physical fact.

The process according to which changes in wave crests occur has been discussed by early investigators, Lake & Yuen (1978), Ramamonjiarisoa & Mollo-Christensen (1979), and Hatori & Toba (1983); the latter two observed 'crest pairing' in wind waves. A related phenomenon is phase reversal in the wave record, which was observed by Melville (1983) always to occur in the neighbourhood of local minima in wave amplitude with breaking present. Detailed studies of these phase jumps by Huang and his colleagues are reviewed by Huang, Long & Shen (1996), who observed in ocean records anomalous phase jumps of 2π magnitude occuring at energy minima, utilizing Hilbert transform processing.

Their accounts of crest loss are consistent with our own raw wave wire records, except that we have also observed crest gain accompanying local upshifting, both with and without wave breaking, but closely correlated with spectral frequency shifts.

The physical length of a wave group is $(2\pi/\delta k)$, and is in our experiments therefore constant in fetch, and a change of ± 1 in the number of waves in a group corresponds to a change of δk in wavenumber. This relation is observed in the present experiment, see figure 9, where a temporary shift in peak energy about $\delta\omega$ (i.e. δk in wavenumber) is observed at 25.2 m, while a concurrent reduction (temporary) in the number of waves from 11 to 10 is also seen. The necessity for the full $\delta\omega$ shift is illustrated in

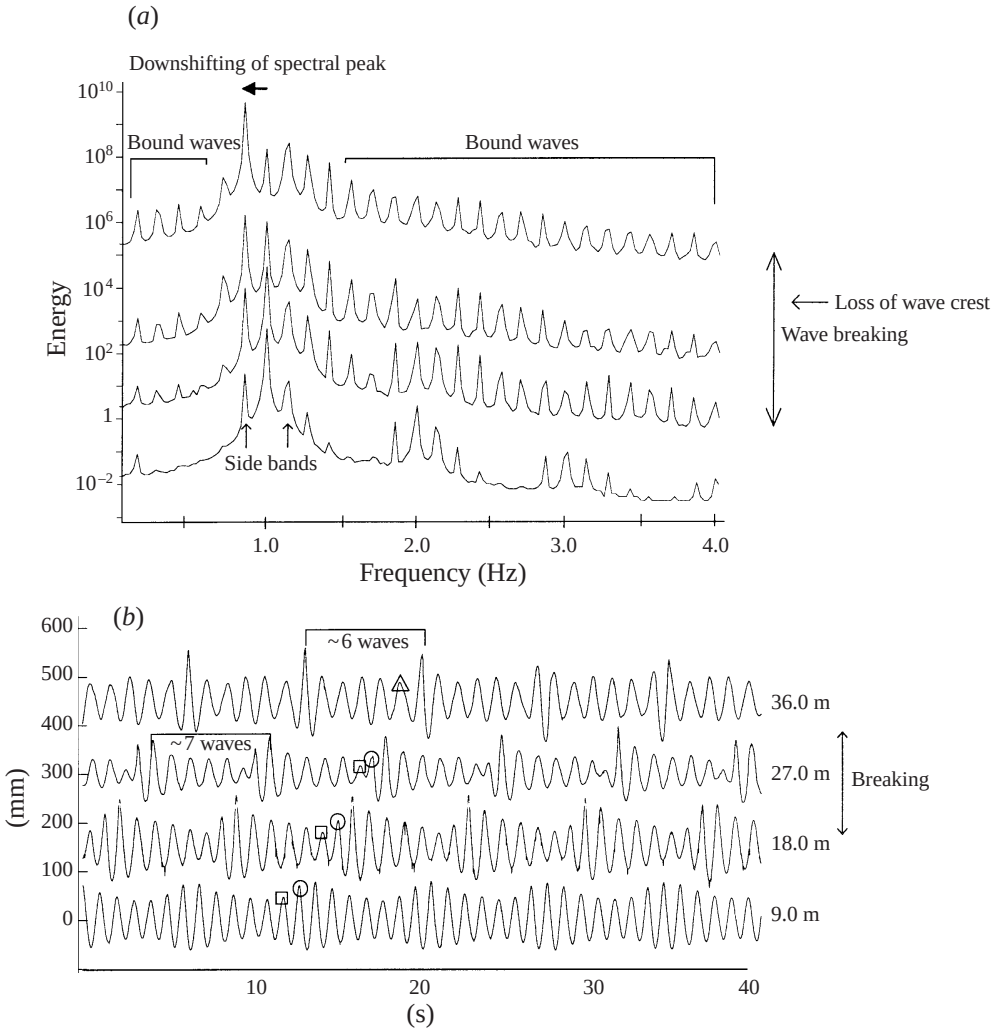

FIGURE 23. Evolution of surface elevation and spectral evolution in fetch, in the case of breaking. In (*b*) the merger of two neighbouring wave crests denoted by □ and ○ into △ is depicted. The spectral evolution (*a*) indicates a full $\delta\omega$ downshifting. The waves are 1.56 m, $\delta\omega/\omega = 0.14$.

figure 20. It seems to have been temporarily reached at fetch 4, where the number of waves is reduced from 9 to 8; however, by fetch 6 the frequency shift has regressed to about $\delta\omega/2$, and the number of waves is back to 9, even though net downshifting has taken place. In another breaking record, figure 23, the loss of a single wave is well correlated with a full $\delta\omega$ downshifting and simultaneous wave breaking.

In these wave records we can on occasion conclude that a wave is in the process of being lost (Yuen & Lake's nomenclature) or of fusing with another wave (Huang's nomenclature) near a region of low wave energy. One example, in which breaking is absent, is in figure 9 at 19.8 m fetch, see the upward arrow; here, the wave train is in the midst of temporary downshifting without breaking. Another example is shown in figure 23 at 27 m fetch where downshifting with breaking is in progress. In this figure, the merging of two neighbouring waves, denoted by □ and by ○ is deduced to occur somewhere between 27 m and 36 m fetch, resulting in the wave denoted by

$\triangle$. It is also between these two fetches that the lower sideband becomes the dominant spectral peak, completing a shift of $\delta\omega$ which began at the first fetch. Based on the evidence in our own wave records, it seems likely that regions of near disappearing wave energy are signatures of wave crest change accompanying frequency shifting, which is itself brought about by complex processes, such as are discussed in § 5.3, and about which much remains to be discovered.

6. Concluding remarks

Experiments on wave instability and its consequences are demanding in terms of facility size, wave generators, and experimental technique and analysis. Pertinent systematic experiments have lagged behind, in quantity, theoretical and numerical studies; this, despite the difficulties faced by the latter in modelling real effects. In addition, the experimental results so far obtained are very limited because of the demand on tank length. Most important, there are no systematic studies which have been able to study evolution beyond one cycle, whether breaking or not. There are, as yet, no studies including the effects of wind either.

Here we have been able to consolidate and extend earlier pioneering studies of the evolution of the BF instability over one cycle, utilizing longer waves and lower steepnesses. This has resulted in the clarification of important issues such as regimes of breaking, the tendency toward recurrence, the effect of breaking on downshifting, high-frequency discretized energy, and the generation of continuous spectra. Clearly, it would be highly desirable to extend these systematic experiments to beyond the first cycle of evolution. As we have commented herein, the quantization of the initial energy in two roughly equal waves at the end of the first cycle suggests a very different and probably faster evolution to follow in the second and succeeding cycles.

Theory discussed here suggests a simple direct relationship between rate of downshifting, and breaking and momentum loss acting together, with near-neighbour energy transfer, the latter due to detuned resonance acting over a limited time (less than 50 wave periods). This is a very different point of view than is commonly incorporated in large-scale wave prediction modelling, and only reinforces the need for further research in this area.

The scientific motivation for understanding the long term evolution of wave groups including real effects would seem clear. There is added motivation provided by the fact that low-grazing-angle radar imaging of wind-driven wave groups (Werle 1995; Smith, Poulter & McGregor 1996; Lamont-Smith, Fuchs & Tulin 1998), provides powerful evidence of their actual existence. This lends strong support to previous contentions as to their importance for ocean processes.

Finally, a variety of wave breaking phenomena which occur in the ocean would seem best modelled in the laboratory through the use of waves breaking in wave groups. We now do this regularly in the OEL, using knowledge gained in these studies. Among these are studies of low-grazing-angle radar scattering from breaking waves (sea spikes), see Fuchs *et al.* (1997), floating bridge wave loadings, see Welch *et al.* (1996), and ringing loads on elastically mounted cylinders, see Welch *et al.* (1998).

We express our thanks to Mr Dominic Regas and Mr Jörn Fuchs for their assistance in preparing and conducting the experiments, and to Y. Yao and M. Landrini for supplying fully nonlinear computational results. This work was supported by: the Ocean Technology Program of the Office of Naval Research, Thomas Swean jr,

program manager and by the Advanced Sensor Applications Program Support, Donna Kulla, program manager.

REFERENCES

Benjamin, T. B. 1967 Instability of periodic wavetrains in nonlinear dispersive systems. *Proc. R. Soc. Lond.* A **299**, 59–75.

Benjamin, T. B. & Feir, J. E. 1967 The disintegration of wave trains on deep water. Part 1. Theory. *J. Fluid Mech.* **27**, 417–430.

Bliven, L. F., Huang, N. E. & Long, S. R. 1986 Experimental study of the influence of wind on Benjamin–Feir sideband instability. *J. Fluid Mech.* **162**, 237–260.

Bonmarin, P. & Ramamonjiarisoa, A. 1985 Deformation to breaking of deep water gravity waves. *Exps. Fluids* **3**, 11–16.

Chu, V. H. & Mei, C. C. 1970 On slowly-varying Stokes waves. *J. Fluid Mech.* **41**, 873–887.

Dold, J. W. & Peregrine, D. H. 1986 Water-wave modulation. *Coast. Engng* 163–175.

Dommermuth, D. & Yue, D. 1987 A high-order spectral method for the study of nonlinear gravity waves. *J. Fluid Mech.* **184**, 267–288.

Dysthe, K. B. 1979 Note on a modification to the nonlinear Schrödinger equation for application to deep water waves. *Proc. R. Soc. Lond.* A **369**, 105–114.

Fuchs, J., Welch, S., Waseda, T., Regas, D. & Tulin, M. P. 1997 Inside the sea-spike: Low grazing angle radar imaging of laboratory waves repeatedly breaking in wave groups. *IGARSS '97*, pp. 714–718. IEEE.

Hammack, J. L. & Henderson, D. M. 1993 Resonant interactions among surface water waves. *Ann. Rev. Fluid Mech.* **25**, 55–97.

Hara, T. & Mei, C. C. 1991 Frequency downshift in a narrowbanded surface waves under the influence of wind. *J. Fluid Mech.* **230**, 429–477.

Hatori, M. & Toba, Y. 1983 Transition of mechanically generated regular waves to wind waves under the action of wind. *J. Fluid Mech.* **130**, 397–409.

Huang, N. E., Long, S. R. & Shen, Z. 1996 The mechanism for frequency downshift in nonlinear wave evolution. *Adv. Appl. Mech.* **32**, 59–117.

Jessup, A. T., Zappa, C. J., Loewen, M. P. & Hesany, V. 1997 Infrared remote sensing of breaking waves. *Nature* **385**, 52–55.

Krasitskii, V. P. 1994 On reduced equations in the Hamiltonian theory of weakly nonlinear surface waves. *J. Fluid Mech.* **272**, 1–20.

Lake, B. M. & Yuen, H. C. 1977 A note on some nonlinear water-wave experiments and the comparison of data with theory. *J. Fluid Mech.* **83**, 75–81.

Lake, B. M., Yuen, H. C., Rungaldier, H. & Ferguson, W. E. 1977 Nonlinear deep-water waves: theory and experiment. Part 2. Evolution of a continuous wave train. *J. Fluid Mech.* **83**, 49–74.

Lake, B. R. & Yuen, H. C. 1978 A new model for nonlinear wind waves. Part 1. Physical model and experimental evidience. *J. Fluid Mech.* **88**, 33–62.

Lamont-Smith, T., Fuchs, J. & Tulin, M. P. 1998 Laboratory investigation of LGA scattering from wind-generated waves and wave groups. *IGARSS '98*, pp. 1219–1221.

Landrini, M., Oshri, O., Waseda, T. & Tulin, M. P. 1998 Long time evolution of gravity wave systems. In *Proc. 13th Intl Workshop on Water Waves and Floating Bodies* (ed. A. J. Hermans), Alphen aan den Rijn, pp. 75–78.

Lo, E. & Mei, C. C. 1985 A numerical study of water-wave modulation base on a higher-order nonlinear Schrödinger equation. *J. Fluid Mech.* **150**, 395–416.

Longuet-Higgins, M. S. 1978 The instabilities of gravity waves of finite amplitude in deep water I. Superharmonics. *Proc. R. Soc. Lond.* A **360**, 471–488.

Longuet-Higgins, M. S. 1980 Modulation of the amplitude of steep wind waves. *J. Fluid Mech.* **99**, 705–713.

Melville, W. K. 1982 The instability and breaking of deep-water waves. *J. Fluid Mech.* **115**, 165–185.

Melville, W. K. 1983 Wave modulation and breakdown. *J. Fluid Mech.* **128**, 489–506.

Oshri, O. 1996 Frequency downshifting in surface waves and free surface flows without waves, PhD thesis, University of California, Santa Barbara.

Phillips, O. M. 1967 Theoretical and experimental studies of gravity wave interactions. *Proc. R. Soc. Lond.* A **299**, 104–119.

Ramamonjiarisoa, A. & Mollo-Christensen, E. 1979 Modulation characteristics of sea surface waves. *J. Geophys. Res.* **84**, 7769–7775.

Smith, M. J., Poulter, E. M. & McGregor, J. A. 1996 Doppler radar measurements of wave groups and breaking waves. *J. Geophys. Res.* **101**, 14269–14282.

Stiassnie, M. 1984 Note on the modified nonlinear Schrödinger equation for deep water waves. *Wave motion* **6**, 431–433.

Stiassnie, M. & Shemer, L. 1987 Energy computations for evolution of class I and II instabilities of Stokes waves. *J. Fluid Mech.* **174**, 299–312.

Su, M.-Y. 1982 Three-dimensional deep-water waves. Part 1. Experimental measurement of skew and symmetric wave patterns. *J. Fluid Mech.* **124**, 73–108.

Su, M.-Y., Bergin, M., Marler, P. & Myrick, R. 1982 Experiments on nonlinear instabilities and evolution of steep gravity-wave trains. *J. Fluid Mech.* **124**, 45–72.

Su, M.-Y. & Green, A. W. 1985 Wave breaking and nonlinear instability coupling. In *The Ocean Surface* (ed. Y. Toba & H. Mitsuyasu), pp. 31–38. D. Reidel.

Trulsen, K. 1989 Frequency down-shift through self modulation and breaking, a numerical study. Master's thesis, University of Tromso.

Trulsen, K. & Dysthe, K. 1990 Frequency down-shift through self modulation and breaking. In *Water Wave Kinematics* (ed. A. Torum & T. Gudmestad), pp. 561–572. Kluwer.

Tulin, M. P. 1996 Breaking of ocean waves and downshifting. In *Waves and Nonlinear Processes in Hydrodynamics* (ed. J. Grue, B. Gjevik & J. E. Weber), pp. 117–196. Kluwer.

Tulin, M. P., Yao, Y. & Wang, P. 1994 The simulation of the deformation and breaking of ocean waves in wave groups. *BOSS'94*, Boston-Ma, pp. 383–392.

Ursell, F. 1952 Edge waves on a sloping beach. *Proc. R. Soc. Lond.* A **214**, 79–97.

Waseda, T. 1997 Laboratory study of wind- and mechanically-generated water waves, PhD thesis, University of California, Santa Barbara.

Welch, S. M., Levi, C., Fontaine, E. & Tulin, M. P. 1998 Experimental loads on a flexibly mounted vertical cylinder in breaking wave groups. *Proc. Eighth* (*1998*) *Intl Offshore and Polar Engineering Conf.* Vol. 1, pp. 178–183. International Society of Offshore and Polar Engineers.

Welch, S., Yao, Y., Tulin, M. P. & Jagannathan, S. 1996 An experimental and numerical investigation of wave loads on floating bridges, including nonlinear and wind effects. *Proc. Sixth* (*1996*) *Intl Offshore and Polar Engineering Conf.* Vol. III, pp. 228–236. International Society of Offshore and Polar Engineers.

Werle, B. 1995 Sea backscatter, spikes and wave group observations at low grazing angles. *IEEE Intl Radar Conf*, pp. 187–195.

Yao, Y. 1992 Theoretical and experimental studies of wavemaking by a large oscillating body in long tanks, including nonlinear phenomena near resonance, PhD thesis, University of California, Santa Barbara.

Yao, Y., Tulin, M. P. & Kolaini, A. R. 1994 Theoretical and experimental studies of three-dimensional wavemaking in narrow tanks, including nonlinear phenomena near resonance. *J. Fluid Mech.* **276**, 211–232.

Yuen, H. C. & Lake, B. M. 1980 Instabilities of waves on deep water. *Ann. Rev. Fluid Mech.* **12**, 303–334.

Yuen, H. C. & Lake, B. M. 1982 Nonlinear dynamics of deep-water gravity waves. *Adv. Appl. Mech.* **22**, 67–229.

Zakharov, V. E. 1968 Stability of periodic waves of finite amplitude on the surface of deep fluid. *J. Appl. Mech. Tech. Phys.* **2**, 190–194.